# INTERIM REPORT I

on

# The Influence of Polarization on Millimeter Wave Propagation through Rain

PARIS H. WILEY, C. W. BOSTIAN,
and W. L. STUTZMAN

Submitted To: National Aeronautics and Space Administration
Washington, D. C.

NASA GRANT NUMBER NGR-47-004-091

June 15, 1973



Electrical Engineering Department
Virginia Polytechnic Institute and State University
Blacksburg, Virginia 24061

## FOREWORD

This document was originally submitted by Paris H. Wiley to the Graduate School of Virginia Polytechnic Institute and State University as a doctoral dissertation. The research it describes was supported by NASA under Grant NGR 47-004-091 and it is being distributed by that project as an interim report.

TABLE OF CONTENTS

## LIST OF ILLUSTRATIONS

# SECTION I

## INTRODUCTION

Weather--especially precipitation--is a major consideration in the design of millimeter wave communications systems. Attenuation and depolarization caused by rainfall, although present at lower frequencies, become the dominant factors affecting propagation along a ground path at frequencies above 12 GHz. A clearer understanding of these weather induced phenomena is essential so that future communications systems can be designed for maximum reliability and economy. Although attenuation has received a great deal of attention in the past 30 years, the influence of polarization on millimeter wave propagation has been ignored until very recently. Practical questions which need to be considered relating to polarization effects are the following: (1) does a polarization exist for which the average attenuation during rainfall is a minimum? (2) What two orthogonal polarizations exhibit the least cross polarization interference? (3) Can polarization diversity be used to increase the reliability of a communications system by using two polarizations which do not fade simultaneously?

This thesis treats the influence of polarization on millimeter wave propagation from both an experimental and a theoretical viewpoint and provides answers to the questions listed above. It first discusses previous theoretical and experimental work relating to the attenuation and depolarization of millimeter waves by rainfall. Considerable detail

is included in the literature review so that the significance of the present work can be judged accurately. Next, a new theoretical model is developed to predict the cross polarization level during rainfall from the path average rain rate and the scattered field from a single raindrop. Finally, data from the VPI&SU depolarization experiment are presented as verification of the new model, and a comparison is made with other theories and experiments.

Several features of the new theoretical model deserve mention here. The attenuation and cross polarization level are computed directly in terms of the scattered fields from the ensemble of raindrops. It does not depend on the difference between the attenuation of vertically and horizontally polarized waves (differential attenuation) to predict the cross polarization level during rainfall. Hence, the validity of the differential attenuation model is checked theoretically. In addition, the other theories which employ scattering and absorption cross-sections or effective propagation constants to predict attenuation are also checked. Unique aspects of the new model are: (1) spherical rather than plane waves are assumed, (2) the average drop diameter is used rather than a drop size distribution, and (3) it is simple enough so that the effect which changing one or more parameters has on the cross-polarization level is easily seen.

## SECTION II

## REVIEW OF THE LITERATURE

### 2.1 Review of theoretical work

Gustav Mie laid the foundation for theoretical work relating to the attenuation and depolarization of electromagnetic waves propagating through rain in 1908. He treated the scattering and attenuation of a plane wave by an ensemble of spherical particles of any material. The method of Mie was first applied to a rain-filled space by Ryde [2] and [3] during World War II. Ryde assumed that all the raindrops are spherical with the same diameter and that the rain is uniform. Medhurst [4], in a later review of Ryde's work, expressed attenuation as

$$\text{Attenuation} = 4.343 \frac{N\lambda^2}{2\pi} A_i \, 10^5 \text{ dB/km}$$

where, N = number of drops per cubic centimeter

$\lambda$ = wavelength in centimeters

$A_i$ = real part of $\sum_{n=1}^{\infty} (a_n + p_n)$

The functions $a_n$ and $p_n$ are computed in terms of the drop parameters and involve Bessel functions of the first kind of order n + 1/2. Although Medhurst [4] corrected several errors made by Ryde [3], attenuations computed using this method do not agree well with measurements. Measured values of attenuation tend to be well above those predicted by the theory.

In addition to its failure to predict attenuation accurately, the approach used by Mie and Ryde says nothing about depolarization due to rainfall. Mie assumed that raindrops are spherical and spherical drops produce no depolarization. In order to predict depolarization it is

necessary to consider that real raindrops tend to be flattened in the vertical direction, and that they resemble oblate spheroids rather than spheres.

The oblateness of the falling raindrops was considered for the first time by Oguchi [5] in 1960. He assumed that the eccentricity (ratio of the axes) of the spheroids was small and considered the oblate raindrop to be a perturbation of the spherical drop. He obtained the first-order change in the scattered field from an oblate raindrop by expanding the scattered field directly in a series of spherical vector wave functions involving powers of the eccentricity ratio $\nu$. Using the geometry shown in Fig. 2.1-1, Oguchi expressed the surface of the spheroid as

$$r = f(\theta) = \frac{a}{\sqrt{1-\nu \sin^2 \theta}}$$

where $\nu = 1 - \frac{a^2}{b^2}$

$\nu < 0$, prolate spheroid

$\nu > 0$, oblate spheroid

Then assuming that the condition

$$|\nu| << 1$$

held for the oblate raindrops (a condition he later found did not hold for the larger drops) he neglected all powers of $\nu$ above the first in his expansion of the scattered fields. The result was a solution for the scattering from an oblate raindrop which gave usable results at least for small and medium sized drops.

The next question which arises is how to extend the solution for a single raindrop to the actual situation of interest in which there are many drops in the propagation path between the transmitter and receiver.

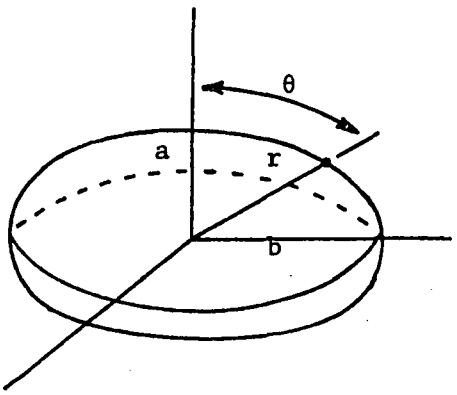


$$r = f(\theta) = \frac{a}{\sqrt{1-\nu \sin^2 \theta}}$$

where $\nu = 1 - \frac{a^2}{b^2}$

$\nu < 0$, prolate spheroid

$\nu > 0$, oblate spheroid

$|\nu| << 1$

Figure 2.1-1. Geometry used by Oguchi in his solution for the scattered field from an oblate raindrop.

Oguchi [5] and [6] used two different approaches to this problem. The first approach [5] was to consider the power removed from the incident field by a single raindrop and then sum over all the drops in a cubic meter in order to obtain the power removed per meter of path length. He defined the total cross section, $Q_t$, of a single drop as

$$Q_t = \frac{\text{total power removed from field}}{\text{Poynting vector of incident field}}$$

For each raindrop $Q_t$ will consist of two parts: one part involving power absorbed in the drop and the other involving power scattered from the drop. Hence,

$$Q_t = Q_a + Q_s$$

and the total cross section is the sum of an absorption cross section and a scattering cross section. The extension to many drops is made by first finding the sum of the cross sections for all the drops in a cubic meter for a given rain rate. Denoted by $\langle Q \rangle$ this equivalent cross section, with units of meter$^2$ per meter$^3$ or meter$^{-1}$, is defined by

$$\langle Q \rangle = \int_0^\infty Q_t(a) \cdot n(a) \cdot da \quad \text{meter}^{-1}$$

where $n(a)da$ is the number of drops per cubic meter which have a drop radius ranging between a and a+ da and $Q_t(a)$ is the corresponding cross section. Evaluation of the above integration requires a knowledge of the drop size distribution as a function of rainfall rate, which Oguchi obtained from Laws and Parsons [7], and a knowledge of terminal velocity as a function of drop radius which he obtained from Best [8]. Then assuming that the same drop distribution is present in every cubic meter along the path and using the standard definition of transmission line

voltage attenuation coefficient, $\alpha$, he derived the attenuation per meter as

$$\alpha = \frac{\text{power lost per unit length}}{2 \cdot \text{incident power at start of unit length}} = \frac{\langle Q \rangle}{2} \text{ meter}^{-1}$$

and therefore,

$$\alpha = 4.343 \times 10^3 \langle Q \rangle \quad \frac{dB}{km}$$

The second approach which Oguchi used [6] in order to extend the single drop solution to the many drop problem was an application of a method published by van de Hulst in his book Light Scattering by Small Particles [9]. This method works with the scattered fields rather than with the power which is absorbed and scattered. An incident plane wave propagating in the +z direction is assumed of the form

$$u_o = S(\theta,\phi) \frac{e^{-jkr}}{jkr}$$

where $S(\theta,\phi)$ is defined as the amplitude function for the raindrop. The jk factor in the denominator is arbitrary and is only inserted by van de Hulst for later convenience. In order to calculate the scattered field from an ensemble of raindrops, Oguchi assumed a plane-parallel slab containing many raindrops as shown in Fig. 2.1-2. All drops are assumed to be identical and identically oriented so that they all have the same amplitude function $S(\theta,\phi)$. The slab has thickness $\ell$ and there are N drops per unit volume. The field at P is influenced by scattering from all the drops in the slab, but the forward traveling wave is influenced coherently only by those drops in the first few central Fresnel zones (drops for which $x^2+y^2 << r^2$). If the distance from the slab to P is large, then the direction is the same from each of the drops in the central Fresnel zones to P and the amplitude function, $S(\theta,\phi) = S(0,0)$,

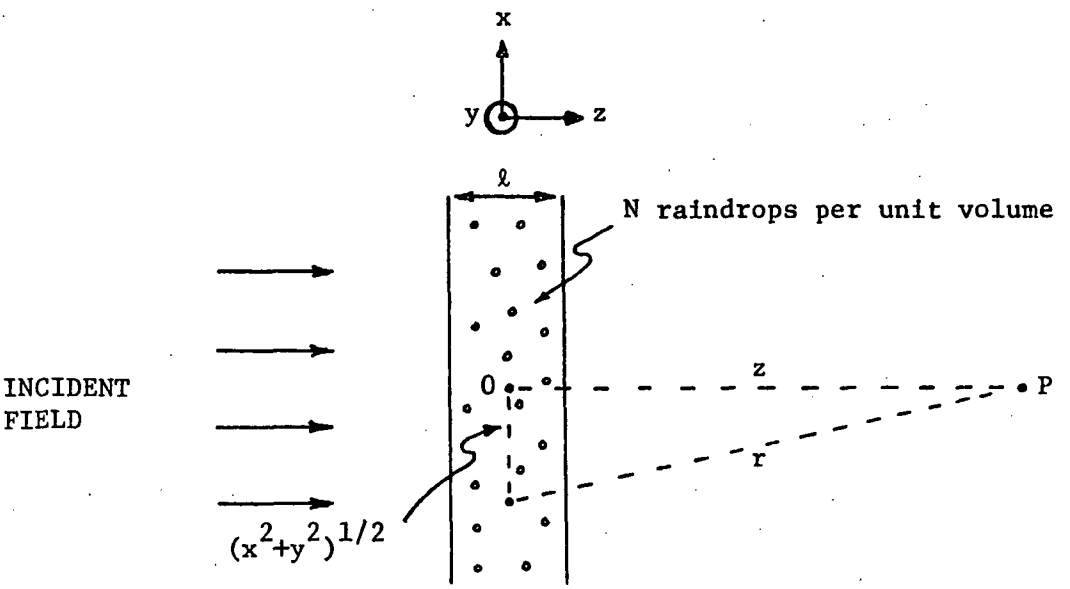


Figure 2.1-2. Oguchi's application of van de Hulst's method to find the attenuation caused by many raindrops.

is the same for all of these drops. The total amplitude at P is then

$$u = u_o \{1 + S(0,0) \int \frac{N}{jkr} e^{-jk(x^2 + y^2)/2r} dx\, dy\, dz\}$$

where the integration is over the entire slab, but where it is assumed the $S(0,0)$ is zero for drops for which the condition $x^2+y^2 << r^2$ does not hold (see van de Hulst [9] page 34). This is a form of Fresnel's integral and can be integrated to give

$$u = u_o \{1 - \frac{2\pi}{K^2} N\ell\ S(0,0)\}$$

This result may be formally represented as the influence of a complex refractive index of the medium as a whole. If the slab is replaced by a slab of homogeneous material with complex refractive index m, m close to 1, the amplitude of the wave is changed by the slab in the proportion

$$e^{-jk\ell(m-1)} = 1 - jk\ell(m-1)$$

Comparing the above equation with the equation for u it is seen that

$$m = 1 - j\ S(0)\ 2\pi\ N\ k^{-3}$$

Separating m into a real part, n, and an imaginary part, n', we have

$$n = 1 + 2\pi\ k^{-3}\ I_m\ \{S(0)\}$$

$$n' = 2\pi\ k^{-3}\ \mathrm{Re}\ \{S(0)\}$$

The real part, n, determines a phase shift of the wave traveling through the rain while the imaginary part, n', determines the attenuation. Oguchi, and more recently Setzer [10], have used this method to compute the attenuation and phase shift of a wave traveling through a rain-filled space. Oguchi [6] has computed the amplitude function $S(\Theta,\Phi)$ for both vertical and horizontal polarization and shown that a

horizontally polarized wave will be attenuated more by rain than will a vertically polarized wave. This is a direct consequence of the oblate shape of the raindrops.

This difference in attenuation between vertically and horizontally polarized waves which Oguchi calculated has been the basis for all theoretical work on rain depolarization to date. Application of Oguchi's results to the depolarization problem was first made by Thomas [11] at Bell Labs, who showed that a difference in attenuation for waves polarized along the major and minor axes of an oblate raindrop would lead to depolarization of any wave not polarized parallel to one of these principal axes. The major and minor axes of the drop are the greater and lesser axes of symmetry of the vertical cross section of the drop, respectively. The depolarization effect is illustrated in Fig. 2.1-3 where $\bar{E}_T$ represents a transmitted wave whose polarization is not parallel to either principal axis. $\bar{E}_T$ can be expressed as a component $\bar{E}_1$ along the major axis and a component $\bar{E}_2$ along the minor axis. As $\bar{E}_1$ and $\bar{E}_2$ propagate, they will be attenuated but their direction will not be changed since they are parallel to the principal axes. $\bar{E}_1'$ and $\bar{E}_2'$ represent $\bar{E}_1$ and $\bar{E}_2$ at the time they reach the receiver. Since $\bar{E}_1$ has been attenuated more than $\bar{E}_2$, $\bar{E}_1'$ will be proportionally smaller than $\bar{E}_2'$ and the resultant $\bar{E}_R$ will not be parallel to $\bar{E}_T$. Hence $\bar{E}_T$ has been depolarized or rotated in the direction of the minor axis of the raindrop. With reference to Fig. 2.1-3 the cross polarization level (XPOL) is computed as follows.

Define, $A_V$ = attenuation of vertically polarized wave

$A_H$ = attenuation of horizontally polarized wave

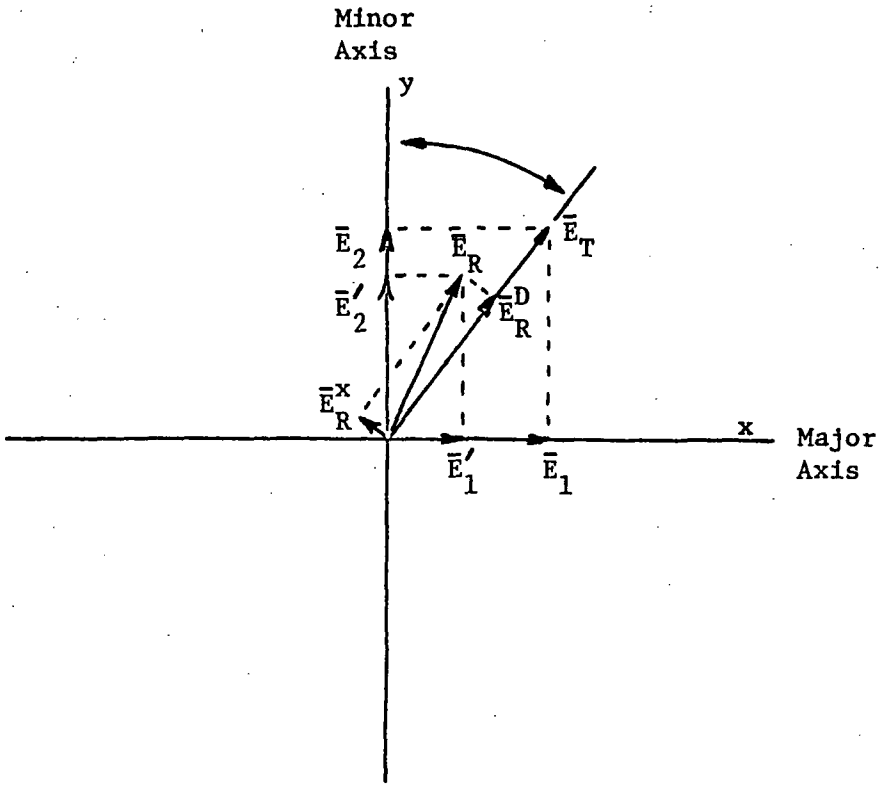


Figure 2.1-3. Depolarization by differential attenuation.

$\eta$ = angle between incident $\bar{E}$ field and vertical

$$E_2' = A_V \, |\bar{E}_T| \cos \eta$$

$$E_1' = A_H \, |\bar{E}_T| \sin \eta$$

$$E_R^D = (A_V \, |\bar{E}_T| \cos\eta \, \hat{y} + A_H \, |\bar{E}_T| \sin\eta \, \hat{x}) \cdot (\cos\eta \, \hat{y} + \sin\eta \, \hat{x})$$

$$= A_V \, |\bar{E}_T| \cos^2 \eta + A_H \, |\bar{E}_T| \sin^2 \eta$$

$$E_R^X = (A_V \, |\bar{E}_T| \cos\eta \, \hat{y} + A_H \, |\bar{E}_T| \sin\eta \, \hat{x}) \cdot (\sin\eta \, \hat{y} - \cos\eta \, \hat{x})$$

$$= A_V \, |\bar{E}_T| \cos \eta \sin \eta - A_H \, |\bar{E}_T| \cos \eta \sin \eta$$

$$\frac{E_R^X}{E_R^D} = \frac{A_V \cos \eta \sin \eta - A_H \cos \eta \sin \eta}{A_V \cos^2 \eta + A_H \sin^2 \eta}$$

$$= \frac{\cos \eta \sin \eta \, (1 - \frac{A_H}{A_V})}{\cos^2 \eta + \frac{A_H}{A_V} \sin^2 \eta}$$

$$= \frac{\cos \eta \sin \eta \, (1 - \frac{A_H}{A_V})}{1 + \sin^2 \eta \, (\frac{A_H}{A_V} - 1)}$$

$$\text{XPOL} = 20 \log_{10} \frac{E_R^X}{E_R^D} = 20 \log 10 \left| \frac{\cos \eta \sin \eta \, (1 - \frac{A_H}{A_V})}{1 + \sin^2 \eta \, (\frac{A_H}{A_V} - 1)} \right|$$

These equations represent the state-of-the-art for computation of the cross polarization level during rainfall. As is now evident, most of the theoretical work has considered attenuation produced by rain rather than depolarization. The differential attenuation model is the only work done to date on the theoretical problem of depolarization and many authors have used it to make quantitative estimates of cross polarization levels. The position of the differential attenuation model is that of any new theory which solves a previously unsolved problem--it must be

proved or disproved by further work. In addition to checking the validity of the differential attenuation model, the new model developed in this thesis overcomes several limitations of the old theory. The most notable contribution is that the cross polarization level is computed directly in terms of the summation of the scattered fields from the ensemble of raindrops rather than being computed indirectly from attenuation predictions. This makes it much easier to see how changing various parameters such as drop size, path length, drop orientation, rain rate, terminal velocity, etc., affect the cross polarization level. The use of a drop size distribution is found to be unnecessary. The uncertainty as to the number of oblate raindrops severely limits accurate prediction of cross polarization and precludes the use of anything other than an average drop size.

The ultimate test of a theoretical model is whether or not it accurately explains experimental observations. In order to correlate theory and experiment, it is imperative that the experimental data be taken under well defined conditions of rainfall rate, drop orientation, etc. The next section discusses the previous experimental work relating to depolarization and it is concluded that no experiment has been performed which serves as more than a crude check of a theoretical model. These experiments must be reviewed in order to point out their limitations and to decide how a depolarization experiment should performed.

## 2.2 Review of experimental work

In 1965, Medhurst [4] published an excellent review of the available

results of experimental attenuation measurements using millimeter waves. He compared the theoretical attenuations computed by Ryde [2] and [3] to experimental data concerning attenuation by rainfall. His conclusion was that "there is a marked tendency for observed attenuations to fall well above levels which, according to the theory, cannot be exceeded." Some of the pre-1965 experiments merit review here in order to learn how such experiments should be conducted.

Typical of the first experiments to measure attenuation due to rainfall was one performed in 1942 by Adam [12]. He used a frequency of 31.25 GHz and a path length of 2 km. He had only one rain gauge along the entire path and it was located at the transmitter end. Semplak [24] found that rain rate can vary as much as 100 mm/hr in a 0.5 km distance and that rain gauge spacing should be less than 0.5 km for accurate rain rate determination. This means that the path average rain rate cannot be inferred from Adam's data making his attenuation measurements of little value. Other early experimenters who used too few rain gauges were Hathaway [13], Rado [14], Okamura [16], and Funakawa [17], and their measured attenuations are equally questionable.

The first experiment utilizing a sufficient number of rain gauges to accurately measure the rainfall rate along the path was conducted in 1947 in Hawaii by Anderson [18]. The frequency used was 24 GHz and the path length was 1.95 km. Nine rain gauges were distributed along the path. Medhurst [4] considers this to be the most carefully performed of any experiment which he reviewed. Figure 2.2-1 shows the data taken by Anderson and it can be seen that the measured attenuation is well above the theoretical curves as calculated by Ryde [3]. This may be

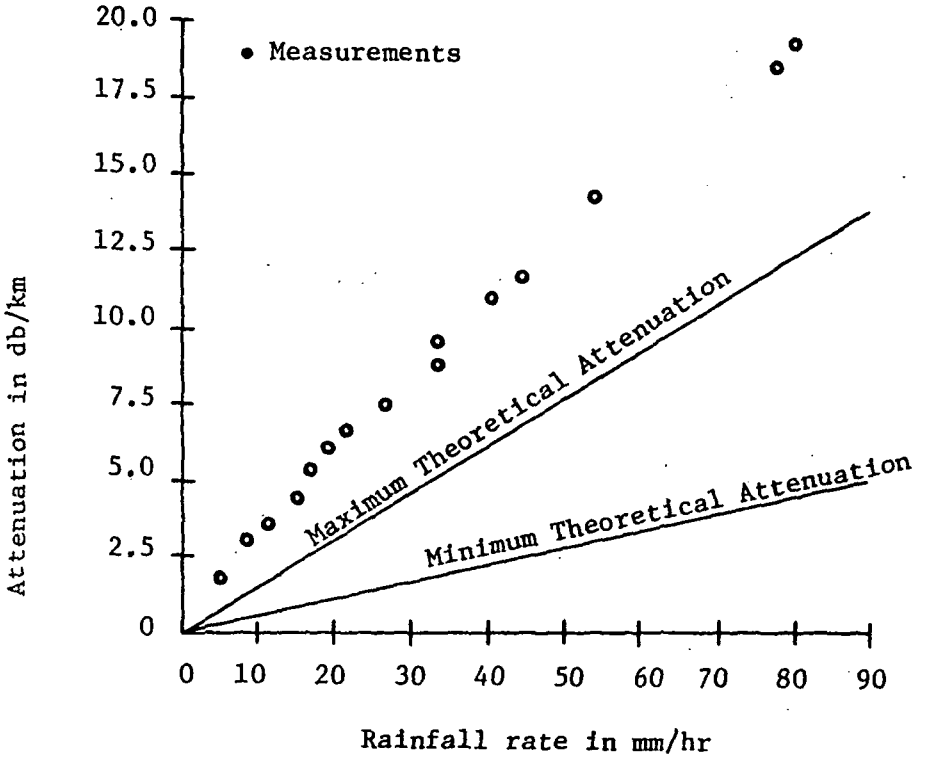


Figure 2.2-1. Measured rainfall attenuation from Anderson [4]

due in part to the tropical climate which produces orographic rain rather than convective thunderstorms.

Perhaps the most advanced measurements of attenuation prior to 1965 were made in 1959 by Okamura [15] at the Radio Research Labs in Tokyo. He used a frequency of 34.884 GHz and a path length of 400 meters. However, a reflection method was used so that the radio wave traversed the path twice making an equivalent path length of 800 meters. One rain gauge was used which was read every 15, 30, or 60 seconds depending on the rainfall rate. The unique feature of Okamura's experiment was that he used both vertical and horizontal polarization, transmitting both during a five minute interval. Figure 2.2-2 shows the attenuation data which he obtained for each polarization. The theoretical limits are from Ryde [6]. As can be seen the attenuation is greater for horizontal polarization then it is for vertical polarization and that both tend to be at or above the maximum possible attenuation as predicted by theory.

In 1967 Semplak [19] began an extensive set of rainfall attenuation measurements covering a period of four years. The first experiment was designed to measure the attenuation of a vertically polarized wave using a frequency of 18.5 GHz and a path length of 6.4 km. Figure 2.2-3 shows the attenuation data which Semplak obtained for a total of 21 storms. The rain gauge spacing of 1.6 km is a possible explanation for the large amount of scatter in the data.

In 1969 Semplak [20] measured the difference between the rainfall attenuation of vertically and horizontally polarized waves using a frequency of 30.9 GHz and a path length of 1.89 km. He transmitted a field polarized at an angle of 45° from the vertical and switched the

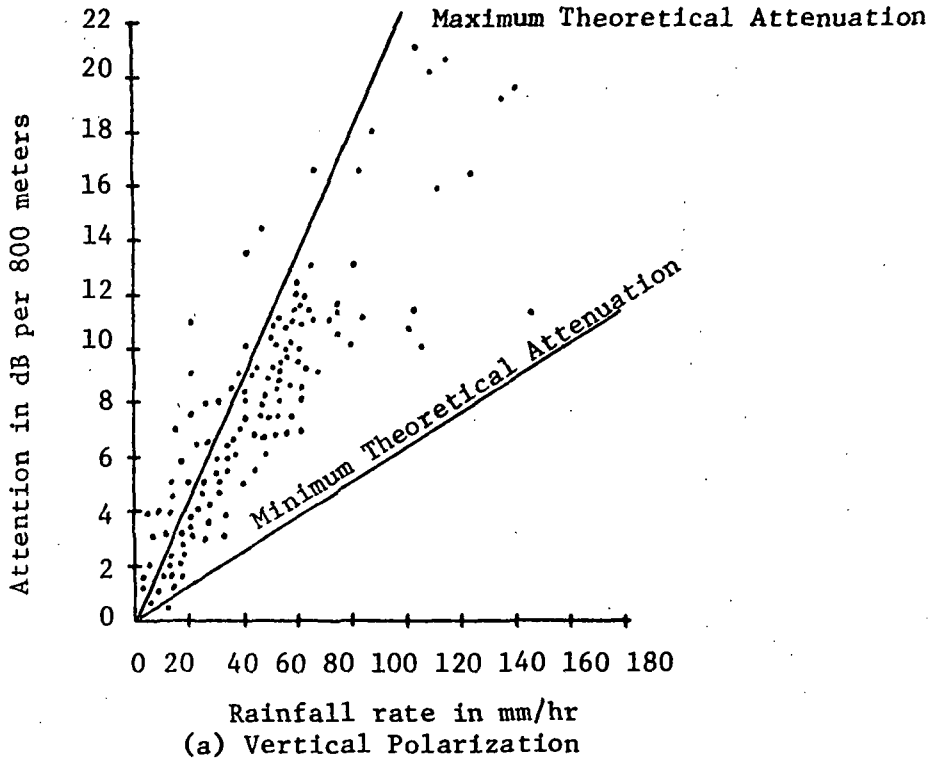


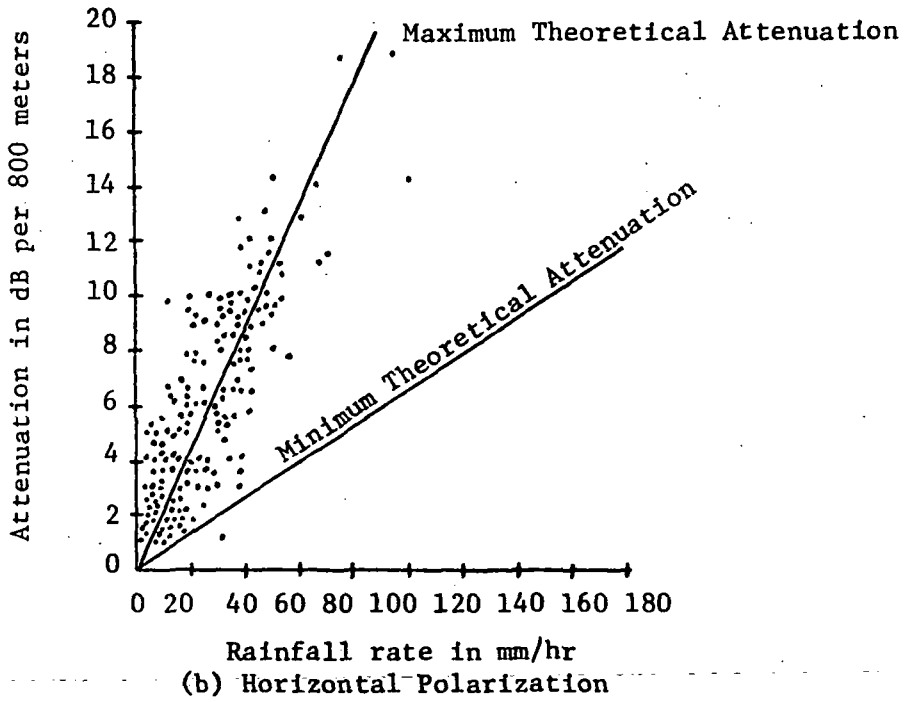


Figure 2.2-2. Measured rainfall attenuation from Okamura [4]

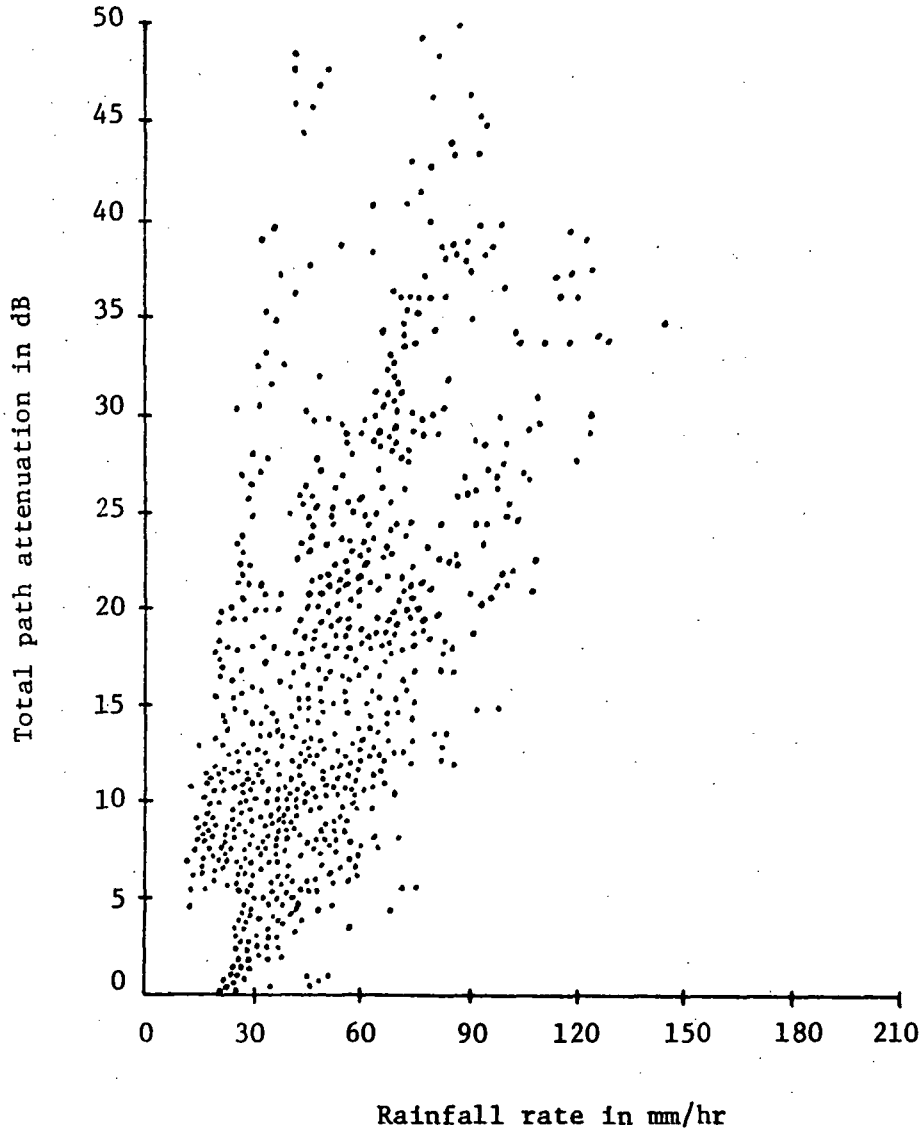


Figure 2.2-3. Measured rainfall attenuation from Semplak for a 6.4 km path at 18.5 GHz [19]

receiving antenna between horizontal and vertical polarization at a rate of 329 Hz using a ferrite switch. He recorded the sum and difference of the horizontal and vertical fields and thus obtained the differential attenuation as a function of total path attenuation. His cumulative data plot is shown in Figure 2.2-4 with horizontal polarization being attenuated more than vertical.

In 1969 Skerjanec and Samson [22] made simultaneous measurements of rainfall attenuation at 10 and 14.43 GHz. They had 20 tipping-bucket rain gauges on a 4.7 km path. Measured attenuation (in dB) at 14.43 GHz was approximately twice that observed at 10 GHz when the rainfall rate exceeded 50 mm/hr. The maximum attenuation observed was 24 dB at 10 GHz and 48 dB at 14.43 GHz corresponding to a rain rate of 137 mm/hr. Readings were recorded only when the rain rate was relatively uniform at all gauges over a selected interval (1-5 min).

In 1970 Semplak [21] made simultaneous measurements of rainfall attenuation at 18.5 and 30.9 GHz. By examining the ratio of the 30.9 GHz attenuation to the 18.5 GHz attenuation during rain, he concluded that the Law and Parsons [7] drop size distribution is adequate to predict the rainfall attenuation observed with terrestrial microwave communications systems.

Since May 1971, Watson [23] at the University of Bradford in England, has been making measurements of attenuation and cross polarization due to rain and snow at a frequency of 11 GHz. He is using ten rain gauges along a 13.5 km path. Initially he transmitted only vertical polarization and employed co-polar and cross-polar antennas at the receiver. Recently a separate horizontally polarized antenna was added at the transmitter

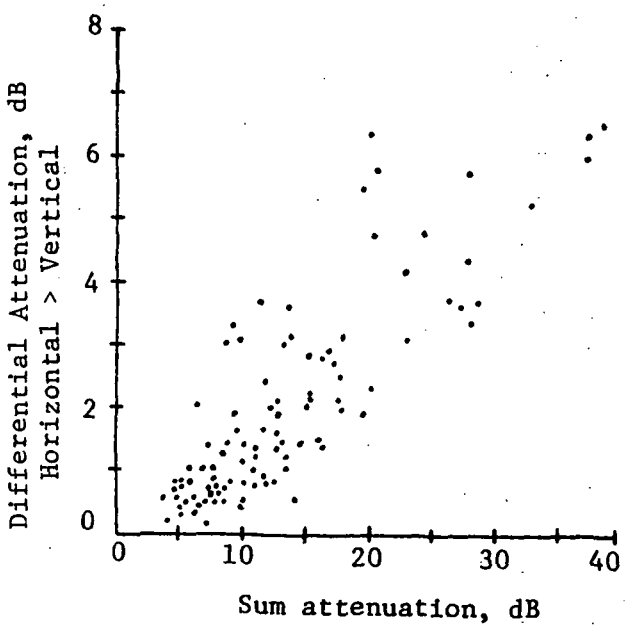


Figure 2.2-4. Measured differential attenuation from Semplak for a frequency of 30.9 GHz and a path length of 1.89 km. [20]

and the polarization transmitted is being switched between vertical and horizontal at 10 Hz. Figure 2.2-5, which is a plot of cross polarization vs. attenuation, is typical of the data which Watson has taken. As can be seen, there is no correlation between the two and, since rainfall rate and attenuation are highly correlated, there can be no correlation between cross polarization and rainfall rate. This is due, as Watson says, to the uncertainty as to the canting angle of the raindrops. Theoretical curves of cross polarization vs. attenuation for canting angles of 5 and 45 degrees are shown in Figure 2.2-5. The problem is that, for a canting angle of zero degrees, the cross polarization isolation is infinite regardless of the attenuation if the transmitted wave is either vertically or horizontally polarized. Hence vertical or horizontal polarization is extremely sensitive to the raindrop canting angle (which is never known). This makes it very difficult to accurately check a theoretical model of cross polarization due to rainfall with data obtained from an experiment using vertical and/or horizontal polarization. The new theoretical model, which will be developed next, predicts the optimum polarization to use for the best correlation of theory to experimental data.

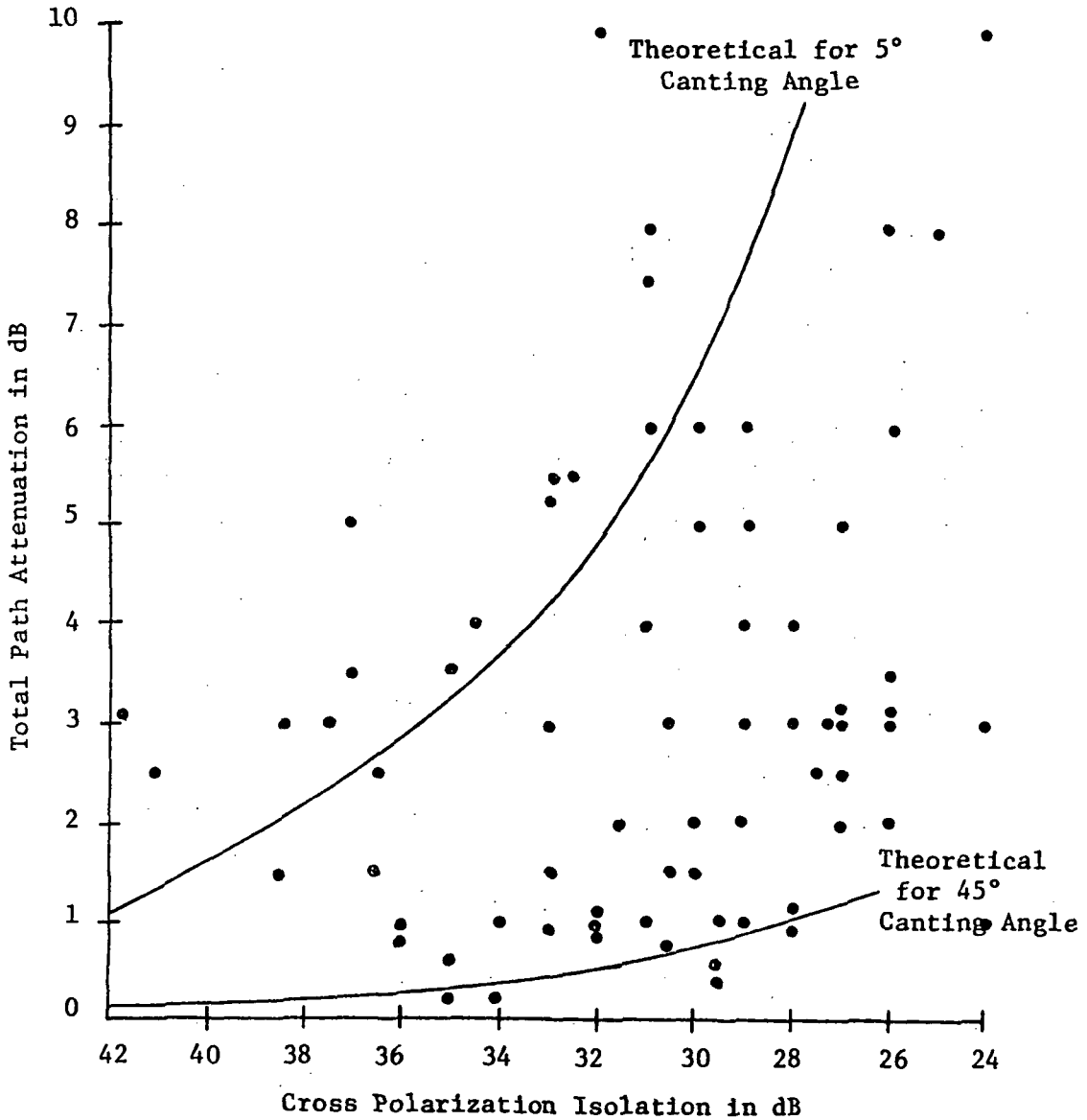


Figure 2.2-5. Measured rainfall attenuation vs. cross polarization from Watson.

## SECTION III

## DEVELOPMENT OF THE THEORETICAL MODEL

### 3.1 Assumptions

Assumptions made in the theoretical model development are: (1) a uniform rain along the path, (2) that all raindrops, regardless of their shape, have the same volume equal to the volume of the most frequently occurring drop, (3) a rain-filled space which is large-scale homogeneous, (4) transmitting and receiving antennas with sufficient beamwidth so that small variations in beamwidth do not affect the received signal (this implies that many Fresnel zones are included in the common volume of the beams), (5) both the incident and scattered fields are spherical waves, and (6) the scattering function for a single drop is known.

### 3.2 An Essential Theorem

Translocation theorem: For a rain cell of width $\Delta\ell$ occurring along a propagation path, the total field at the receiver is independent of the actual position of the cell along the path and depends only on the cell width.

The above theorem is central to the theoretical model development and its validity will be demonstrated first. The technique to be employed is the method of Fresnel zone analysis which has been used extensively in the solution of diffraction problems. Livingston [25] gives a detailed justification for this method which will be reviewed briefly here.

Consider an arbitrary plane perpendicular to the propagation path in a homogeneous medium as shown in Figure 3.2-1. Point O is the intercept of the plane with a straight line connecting the antennas. By Huygen's principle the field at the receiver may be obtained by considering each point in the plane to be the source of a new spherical wave with an amplitude and phase equal to the amplitude and phase of the transmitted field at that point. The total field at the receiver is then the sum of the spherical waves from each point in the plane. The wave from point O will arrive at the receiver first since it travels the shortest distance. The phase of the waves from all other points will lag behind that of the wave from point O, and this phase lag will increase as points farther and farther from O are considered. The locus of points in the plane for which the phase lag is exactly $\pi$ radians determines a circle with center at O and radius $F_1$. This circle defines the boundary of the first Fresnel zone. All points at a distance less than $F_1$ from point O are in the first Fresnel zone. Similarly, circles with radii $F_2$, $F_3$, etc. are defined for phase shifts of exactly $2\pi$, $3\pi$, etc. with the area between $F_1$ and $F_2$ defined as the second Fresnel zone, that between $F_2$ and $F_3$ the third Fresnel zone, etc. The total field at the receiver may be expressed as a summation of the fields from each of the Fresnel zones. Since there is an infinite number of Fresnel zones, an infinite series must be summed. Since the phase of the wave is changing by $\pi$ radians as the summation proceeds from one zone to the next, the signs of the terms of the infinite series alternate. Livingston shows that each of the Fresnel zones has the same area and therefore the same

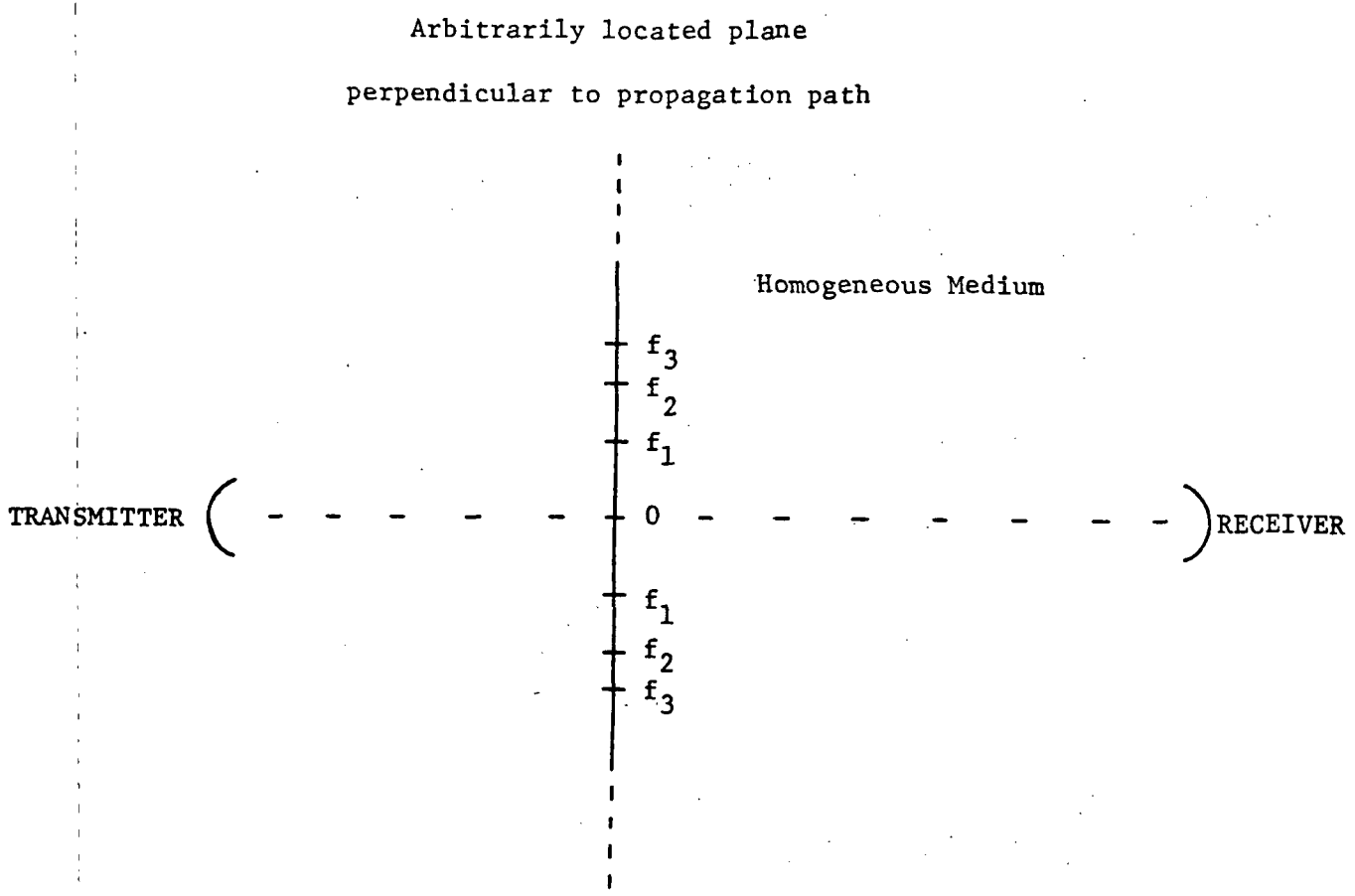


Figure 3.2-1. Definition of Fresnel zones.

number of points to contribute to the field, but the contribution of the outer zones is increasingly smaller due to the greater distance and correspondingly greater free-space loss. The summation of the fields from each of the Fresnel zones is, therefore, the summation of an infinite geometric alternating series. Since the sum of such a series approaches half the value of the first term of the series when the value of its common ratio approaches unity, the total field at the receiver may be found by calculating the contribution of only those points in the first Fresnel zone and taking one-half of the result.

Now for a proof of the theorem, consider the geometry as shown in Figure 3.2-2 where the first Fresnel zone is defined as the locus of points for which the phase lag is $\pi$ radians. The total path length between the transmitter and receiver is L, and $\Delta\ell$ is an elemental length of the path at a distance $\ell$ from the transmitter. $\Delta V$ is the elemental volume defined by $\Delta\ell$ and the boundary of the first Fresnel zone. There is assumed to be rain in the volume $\Delta V$ with no rain along the rest of the path. The radius of the first Fresnel zone at $\ell$ is given by Livingston [25]

$$r = \sqrt{\frac{\lambda \ell (L-\ell)}{L}} \quad \alpha \quad (\ell - \ell^2/L)^{1/2} .$$

The vertical axis in Figure 3.2-2 is greatly expanded relative to the horizontal axis. At 17.65 GHz the radius r is less than one meter at midpath for a path length of 1.43 km. Assuming spherical waves are transmitted, the incident field at the receiver will be inversely proportional to the path length L while the incident field at $\ell$ will be inversely proportional to $\ell$.

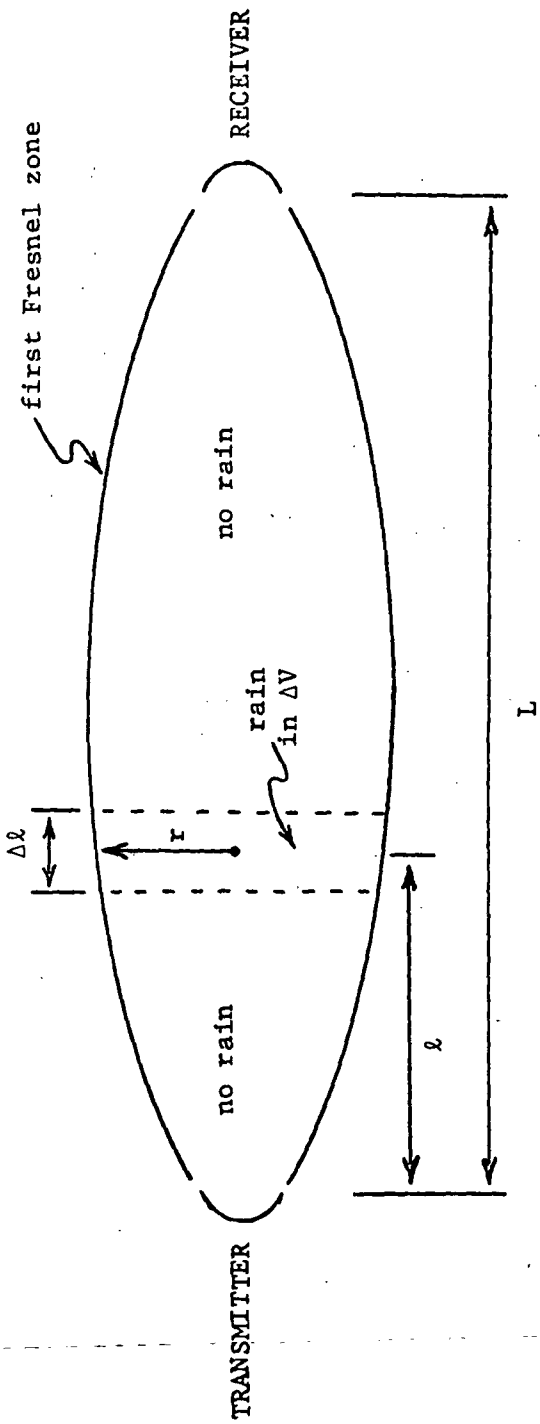


Figure 3.2-2. Geometry Used in Proof of Theorem.

$$E^i_{REC} \alpha 1/L \qquad E^i_\ell \alpha 1/\ell$$

The scattered field at the receiver from the raindrops in the volume $\Delta V$ will be directly proportional to the incident field at $\ell$ and directly proportional to the total number of raindrops in $\Delta V$ which in turn is proportional to $\Delta V$. The scattered field at the receiver will be inversely proportional to the distance $L-\ell$ from $\Delta V$ to the receiver.

$$E^S_{REC} \alpha E^i_\ell \Delta V\left(\frac{1}{L-\ell}\right)$$

$$\alpha \frac{\Delta V}{\ell L-\ell^2} \quad \text{since } E^i_\ell \alpha 1/\ell$$

$$\text{But} \quad \Delta V \alpha r^2 \Delta\ell \alpha (\ell-\ell^2/L)\,\Delta\ell$$

$$\text{Therefore} \quad E^S_{REC} \alpha (\ell-\ell^2/L)\,\Delta\ell \frac{1}{\ell L-\ell^2}$$

$$\alpha \frac{\Delta\ell}{L}(\ell L-\ell^2)\left(\frac{1}{\ell L-\ell^2}\right)$$

$$\alpha \Delta\ell/L$$

$$\text{And} \quad E_{ratio} = \frac{E^S_{REC}}{E^i_{REC}} \alpha \frac{\Delta\ell/L}{1/L} \alpha \Delta\ell$$

Hence the scattered to incident ratio is independent of the position of a rain cell along the path and is independent of the length of the path. It depends only on the width of the rain cell. If rain is falling along the entire path, then $\Delta\ell=L$ and the ratio depends on the path length.

## 3.3 Model Development

### 3.3.1 Path Division

Consider the rain-filled volume bounded by the first Fresnel zone as shown in Figure 3.3.1-1(a). Divide the total number of drops

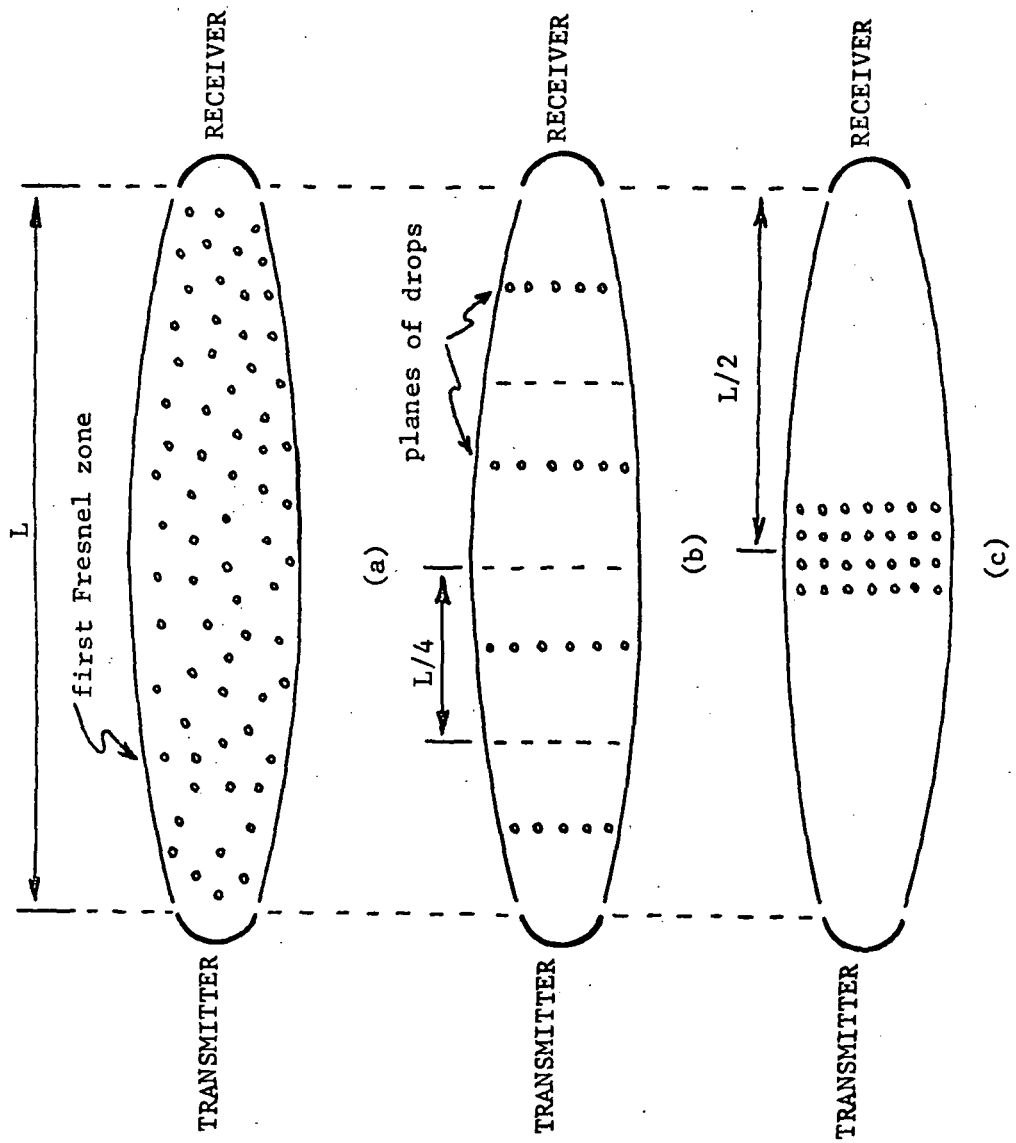


Figure 3.3.1-1. Division of Path When N = 4.

into N groups by dividing the path into N equal segments of length L/N. Place the drops in each group in a plane at the center of each segment as illustrated for N=4 in Figure 3.3.1-1(b). It follows from the translocation theorem of Section 3.2 that the contribution to the scattered field at the receiver is the same for each plane of drops and is independent of the actual position of the plane along the path. However, it must be noted that planes near the center of the path contain more drops than those near the ends since the volume of a segment near the center is larger than the volume of a segment near either end. Moving a plane of drops from one position to another requires changing the number of drops by the ratio of the volumes of segments at the two positions in order to maintain the same contribution to the scattered field at the receiver.

Next assume that all planes are moved to new positions near the center of the path as shown in Figure 3.3.1-1(c). All planes will be at the same distance L/2 from the receiver and all planes must make equal contributions to the scattered field (since they all made equal contributions in their former locations). It follows that all planes must have the same number of drops and are identical. Therefore one need only solve for the scattered field from a single plane.

### 3.3.2 Scattering from a Single Plane

The following complex forward scattering coefficients are defined for a single plane of drops in terms of an incident (main) polarization (1) and an orthogonal (cross) polarization (2). These

coefficients will be the same for all planes.

$S_{11}$ scattered $\bar{E}$ field with polarization (1) produced by an incident $\bar{E}$ field with polarization (1).

$S_{12}$ scattered $\bar{E}$ field with polarization (2) produced by an incident $\bar{E}$ field with polarization (1).

$S_{21}$ scattered $\bar{E}$ field with polarization (1) produced by an incident $\bar{E}$ field with polarization (2).

$S_{22}$ scattered $\bar{E}$ field with polarization (2) produced by an incident $\bar{E}$ field with polarization (2).

The scattered field at the receiver from a single plane of drops can be found by summing the scattered fields from each of the drops in the plane. With reference to Section 3.2 it is necessary to consider only those drops in the first Fresnel zone and to multiply the result by one-half. Oguchi [26] has computed complex forward scattering coefficients for a single raindrop. In terms of forward scattering functions ($f_{pq}$) computed from Oguchi's functions, (see the Appendix) the scattering coefficients for a plane of drops will be of the form

$$S_{pq} = \frac{1}{2} \Sigma E_p^i f_{pq} \frac{e^{-jkr}}{r}$$

where $E_p^i$ is the incident field with polarization p,

$r$ is the distance from the drop to the receiver,

$f_{pq}$ is the ratio of the scattered $\bar{E}$ field with polarization (q) to the incident $\bar{E}$ field with polarization (p) for a <u>single</u> drop,

and where the summation is to be performed over those drops in the first Fresnel zone. The scattering function $f_{pq}$ is assumed constant for all drops in the plane which have the same shape. As discussed in Section 4, the total drop population is assumed to consist of 40% identical oblate drops and 60% identical spherical drops. A constant $f_{pq}$ for all drops of the same shape requires that all oblate drops be identically oriented and that the radius of the first Fresnel zone be very much less than the path length so that only forward scatter need be considered. The r in the denominator of the previous equation may be replaced with L/2 yielding

$$S_{pq} = \frac{E^i_p f_{pq}}{L} \Sigma e^{-jkr}$$

Assuming a uniform distribution of drops within the first Fresnel zone, the above equation is easily evaluated. The result of the summation is an imaginary constant, $K = -j \frac{2}{\pi}$, times the number of drops, D, in the plane (see the Appendix). Hence,

$$S_{pq} = \frac{E^i_p f_{pq}}{L} KD = -j \frac{2}{\pi L} DE^i_p f_{pq}$$

3.3.3 Effect of N Planes

The effect of N planes of drops in series may be found by considering the incident field to interact with the first plane producing a new field which then interacts with the second plane, etc. until all N planes have been considered. This may be expressed in closed form in terms of the scattering coefficients ($S_{pq}$'s). It is assumed that the incident field at midpath has amplitude two so

that the incident field at the receiver has unity amplitude. It is also assumed that the contribution from the $S_{21}$ coefficient (scatter from cross to main polarization) is small and that $S_{21}$ is zero. This is valid for cross polarization levels less than about -5 dB.

As shown in Figure 3.3.3-1, the total fields at the receiver are obtained by induction from the effect of a single plane. After interaction with the first plane of drops the total main polarization field $E_M$ will consist of the sum of the incident field at the receiver (unity) and the scattered field $S_{11}$. The total cross polarization field $E_X$ will consist only of the scattered field $S_{12}$ since the incident field in this polarization is zero. The fields leaving plane 1 then interact with plane 2. The main polarization component will be multiplied by another $(1 + S_{11})$ factor. The cross polarization component will consist of two parts: (1) the previous cross polarized component $E_X$ which will be attenuated by a $(1 + S_{22})$ factor, and (2) a new contribution from the previous $E_M$ equal to $E_M$ times $S_{12}$. This method is continued for all N planes with the following result as shown in Figure 3.3.3-1.

$$E_M = (1 + S_{11})^N$$

$$E_X = S_{12}[(1+S_{22})^{N-1} + (1+S_{22})^{N-2}(1+S_{11}) + \ldots. + (1+S_{22})(1+S_{11})^{N-2} + (1+S_{11})^{N-1}]$$

The above described method forms the basis for the computer program which is listed in the Appendix. This program was used to

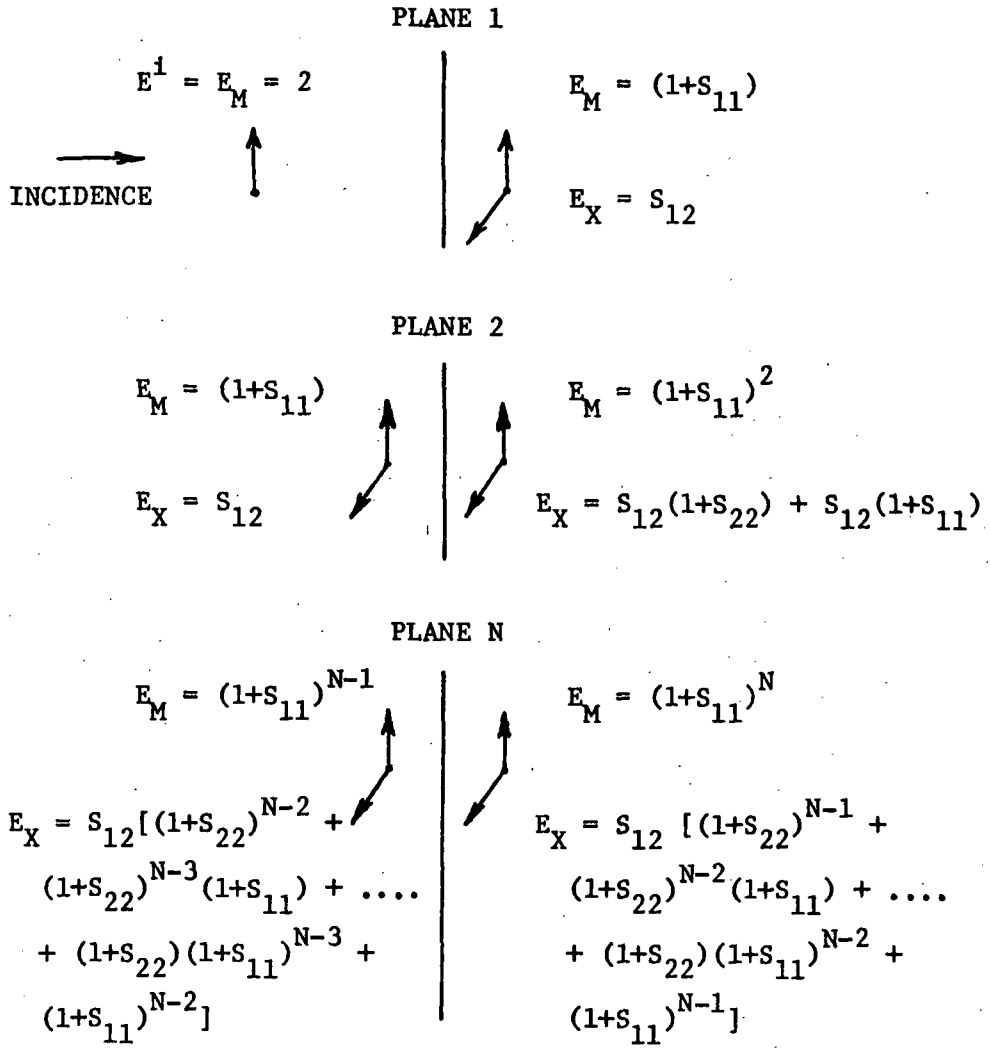


Figure 3.3.3-1. Effect of N planes of drops in series.

make calculations of expected cross polarization and attenuation levels during rainfall which are compared to experimental data from the VPI&SU depolarization experiment in the next section. In Section 5 a comparison is made with other theories and experiments.

## SECTION IV

## EXPERIMENTAL VERIFICATION

### 4.1 VPI&SU Depolarization Experiment

#### 4.1.1 General System Description

The depolarization experiment sponsored by NASA and conducted at Virginia Polytechnic Institute and State University has been described in detail elsewhere [27] and will be reviewed only briefly here. The experiment is designed to measure depolarization and attenuation effects of rainfall on millimeter wave propagation. The path is 1.43 km in length and is located on the VPI&SU campus in Blacksburg, Virginia. The measurements are being made at a frequency of 17.65 GHz with two separate transmit and receive channels orthogonally polarized at $\pm 45°$ from the vertical.

Figure 4.1.1-1 presents a block diagram of the overall experiment. It consists of (1) an RF system (millimeter wave transmitter and receiver), (2) transmitting and receiving antennas (dual polarized), (3) a weather monitoring system with rain gauges and wind sensors, (4) a digital control, processing, and data storage system built around a Raytheon PB 440 computer, and (5) a link via magnetic tape to an IBM 370/155 computing system for off-line data processing.

An important feature of this experiment is the absence of possible multipath effects which could produce cross polarization. The common volume of the main beams of the antennas does not

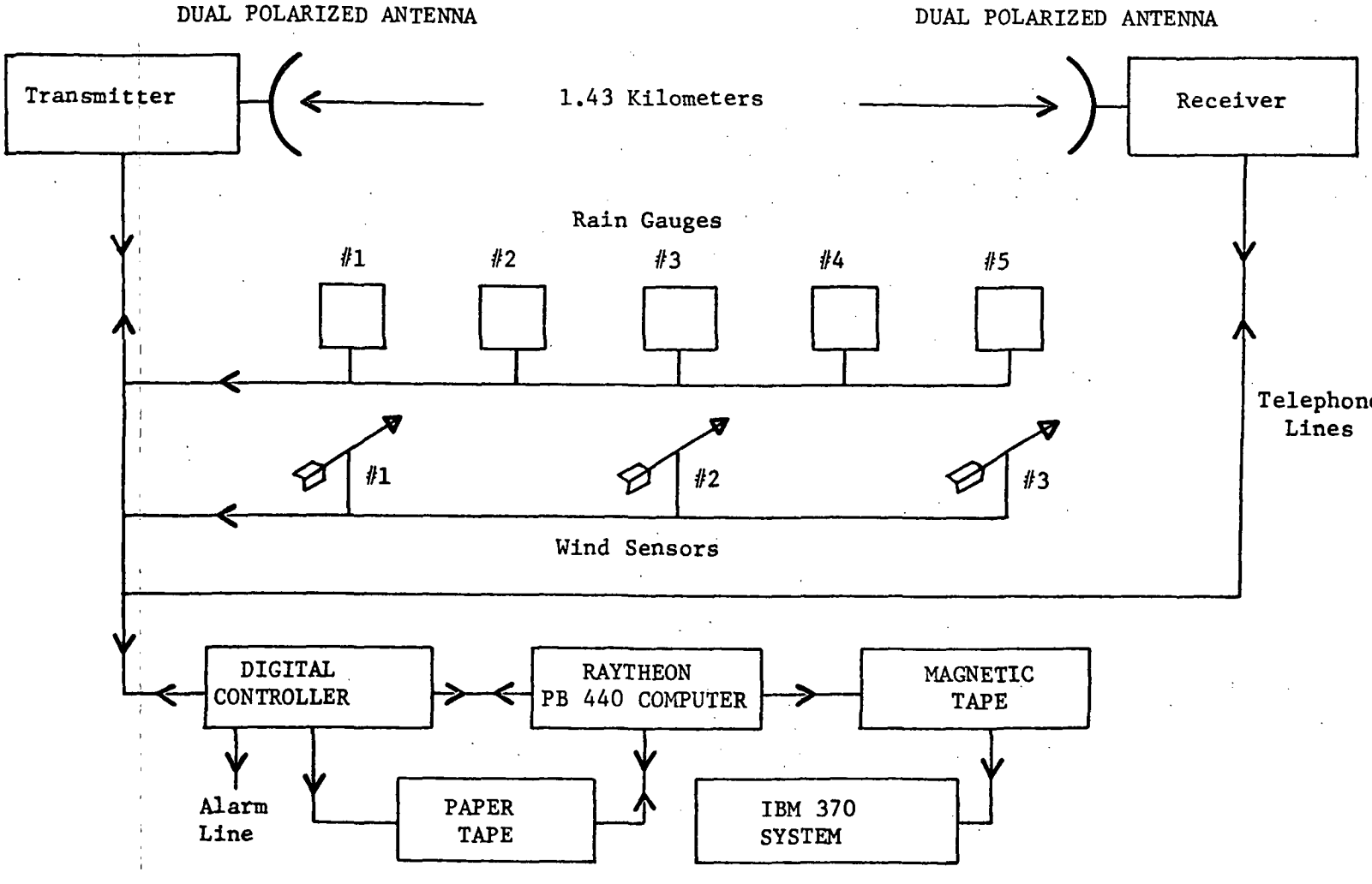


Figure 4.1.1-1. Experiment Block Diagram.

intercept the ground or any other obstacle. The angle to the ground at midpath from either antenna is 2° and the angle from the mainbeam maximum to the first null of the radiation pattern is about 1°. Therefore only sidelobes intercept the ground and any multipath effects are more than 40 dB below the direct signal.

### 4.1.2 Data Processing

#### 4.1.2.1 On-Line Processing

A Raytheon PB 440 computer assisted by a special-purpose controller operates the experiment, acquires data, and does preliminary data processing. The experimental control program maintains the system in the proper operating mode for current weather conditions and signal behavior. The clear weather operating mode is called mode 0, and in it the +45° transmitter channel operates continuously while the computer monitors the +45° to -45° cross polarization level and the +45° direct attenuation. Both receiver channels are sampled at 10 second intervals while wind velocity and transmitter power are sampled every 100 seconds. If the cross polarization level (in dB) changes by more than 2% or if one of the rain gauges reports precipitation, the system begins operating in mode 1. During mode 1 operation, transmission is sequenced at 4 second intervals from the +45° to the -45° channel and then to both channels. Receiver sampling occurs at 1 second intervals and wind velocity is sampled every 4 seconds. Mode 1 operation

continues until the precipitation rate falls below 6 mm/hr or until the cross polarization level stabilizes. At this time, mode 2 operation is begun with transmitter switching at 10 second intervals and receiver and wind sampling at 2 and 10 second intervals respectively. Mode 2 operation continues until the precipitation rate falls below 3 mm/hr. The system then enters mode 3 with transmitter switching at 100 second intervals and receiver and wind sampling at 10 and 100 second intervals respectively. When the precipitation rate falls below 2 mm/hr, the system re-enters mode 0 operation. In all modes there is a low pass filter (time constant = 0.4 seconds) at the input to the A-D converter which surpresses fast scintillations of the signals and insures that average values are sampled.

When a new data point enters the computer, a program locates the last two values stored for that input. If the new value and the last value differ by more than 1% the new value is stored. If the difference between the new value and the last value is less than 1%, the new value is compared to the next to last value. If these differ by more than 1%, the new value is stored; if this difference is less than 1%, the last value is discarded and the new value takes its place.

4.1.2.2 Off-Line Processing

An IBM 370/155 computer program has been developed

which processes, analyzes, and plots the accumulated data from any number of selected storms. These data are rain rates from each gauge plus quasi-instantaneous (i.e. short integration time) samples of the analog signal levels during a storm. The latter are stored at essentially regular times while the intervals between successive rain gauge trips are random. Before data from different inputs can be compared the computer must generate a time-function representation for each variable. These time functions are then averaged over selected time intervals to generate the average signal levels, rain rates, etc., required by steady state theory.

## 4.2 Comparison of Theory and Experiment

The data from the VPI&SU depolarization experiment have been described in detail elsewhere [28]. The intent of this section is to provide a review of the data sufficient to check the validity of the depolarization model developed in Section 3. Experimental results are presented using graphs which also contain theoretical predictions based on the model of Section 3 and calculated using the computer program listed in the Appendix. These figures make the comparison between theory and experiment evident at a glance. The main test of the theory is the accurate prediction of the cross polarization level as a function of rainfall rate and most of the figures are of this type. However, plots of attenuation versus rainfall rate and cross polarization versus attenuation are included since they provide additional support for the model. For all of the data presented here a 15 second time average

(performed off-line) was used for both the rain rate and the received signal levels. In addition, all data points for each integer value of rain rate were averaged to produce a single data point for that rain rate. Standard deviations were also computed for each data point. The range of standard deviations is stated in the text for each figure but it is not plotted since it tends to obscure the data points.

The first storm after the experiment became operational occurred on August 4, 1972. Figure 4.2-1 shows the cross polarization level for this storm. There is considerable scatter in the data but the theoretical curve is certainly representative of the average level observed. The scatter is most likely due to an inaccurate measurement of the rainfall rate since only two raingauges were in operation at the time. As discussed in Section 2.2, an intergauge spacing of 1.43 km is not sufficient for an accurate measurement of rainfall rate. The standard deviation of the data points in Figure 4.2-1 is about 5 dB and all but two points are closer than this to the theoretical curve.

Figure 4.2-2 presents data taken on August 17, 1972. This storm provided most of the data which were taken during 1972. The peak rain rate of 105 mm/hr was the maximum rain rate observed. As can be seen, there is good agreement with the theoretically predicted cross polarization level. Since there were still only two raingauges along the path, scatter is to be expected in this data also. The standard deviation for these points is a little less than 5 dB.

Data from the storm of September 29, 1972 is shown in Figure 4.2-3. There is excellent agreement with theory except for rainrates less than

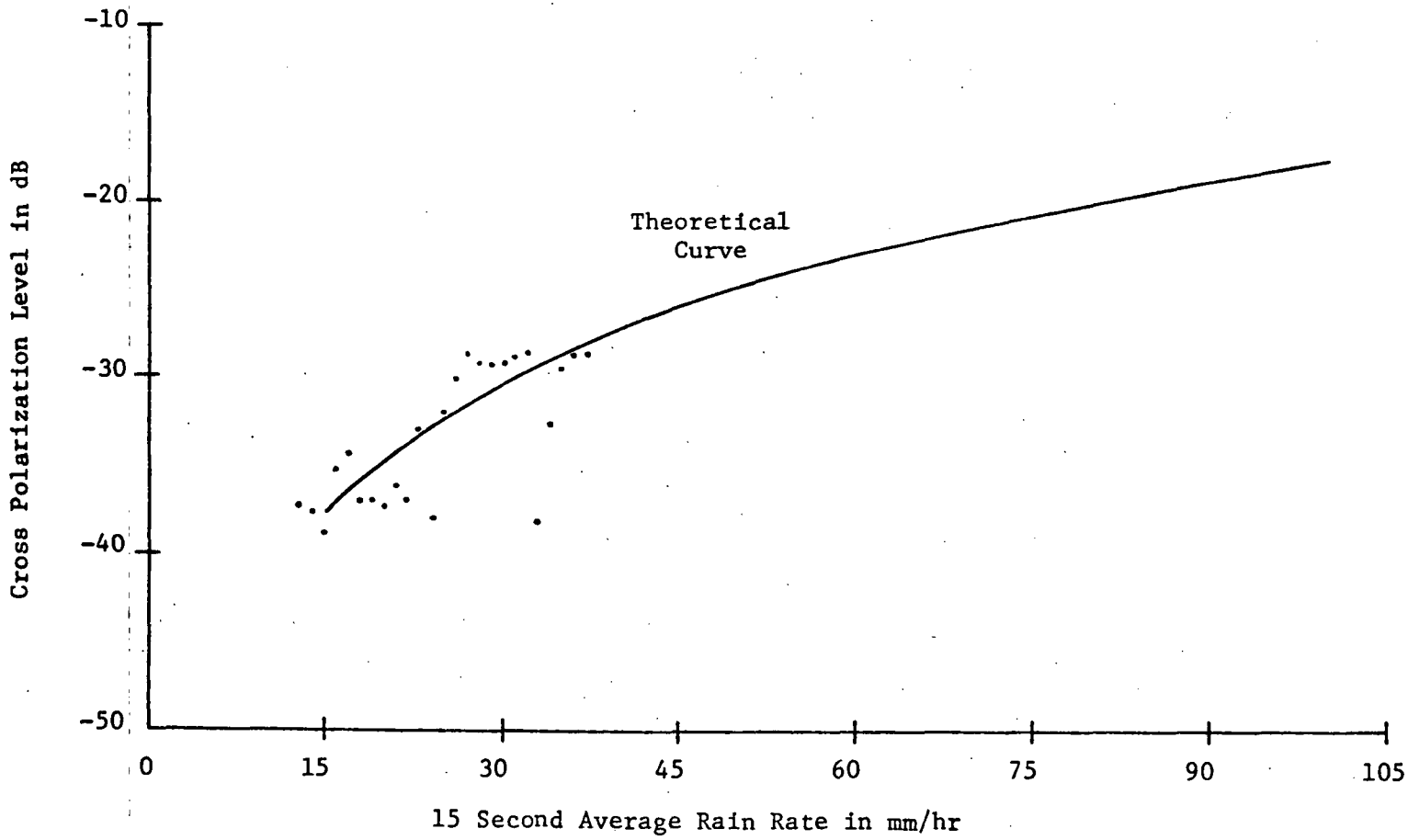


Figure 4.2-1. Average Cross Polarization Level for August 4, 1972.

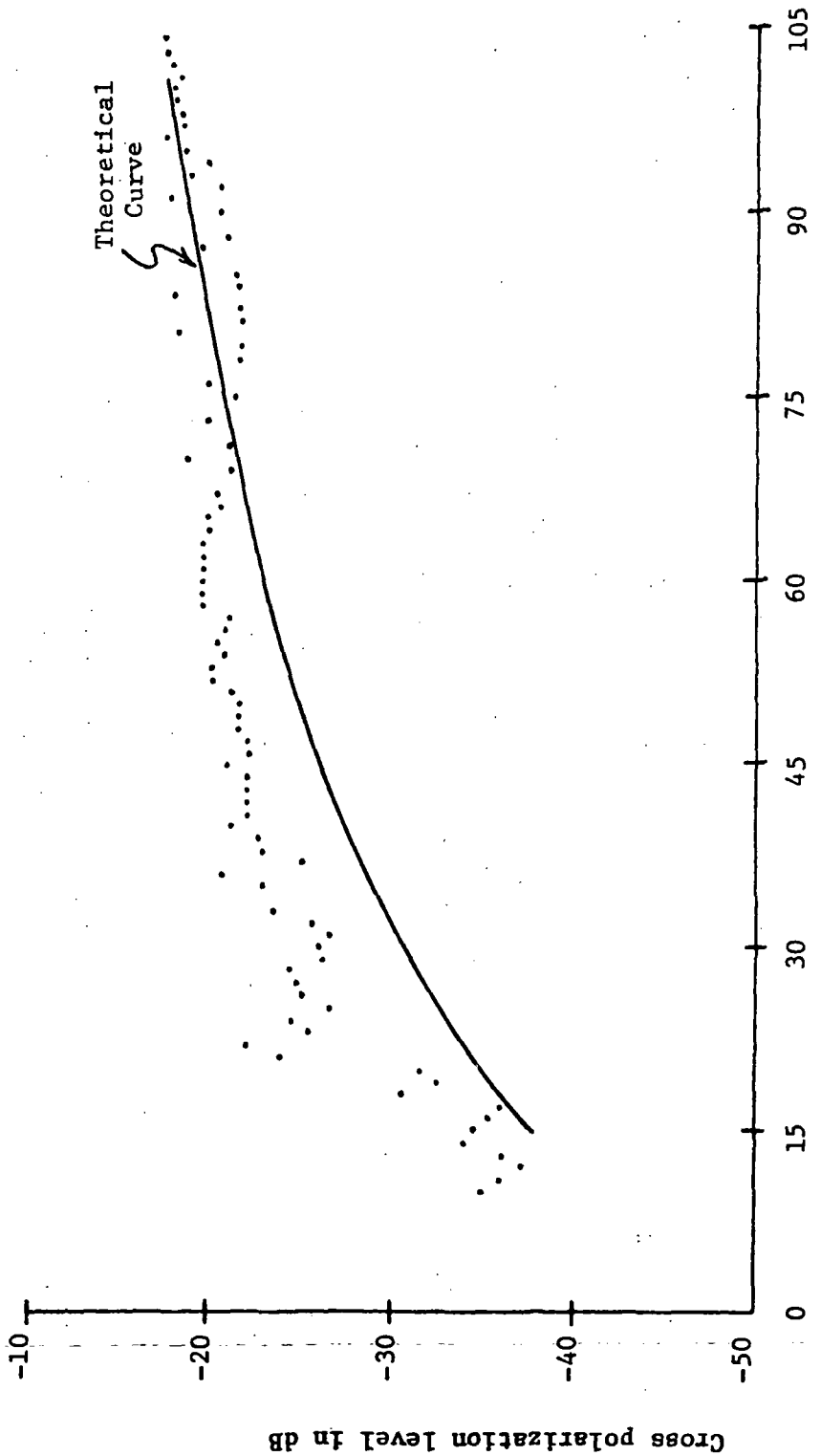


Figure 4.2-2. Average Cross Polarization Level for August 17, 1972.

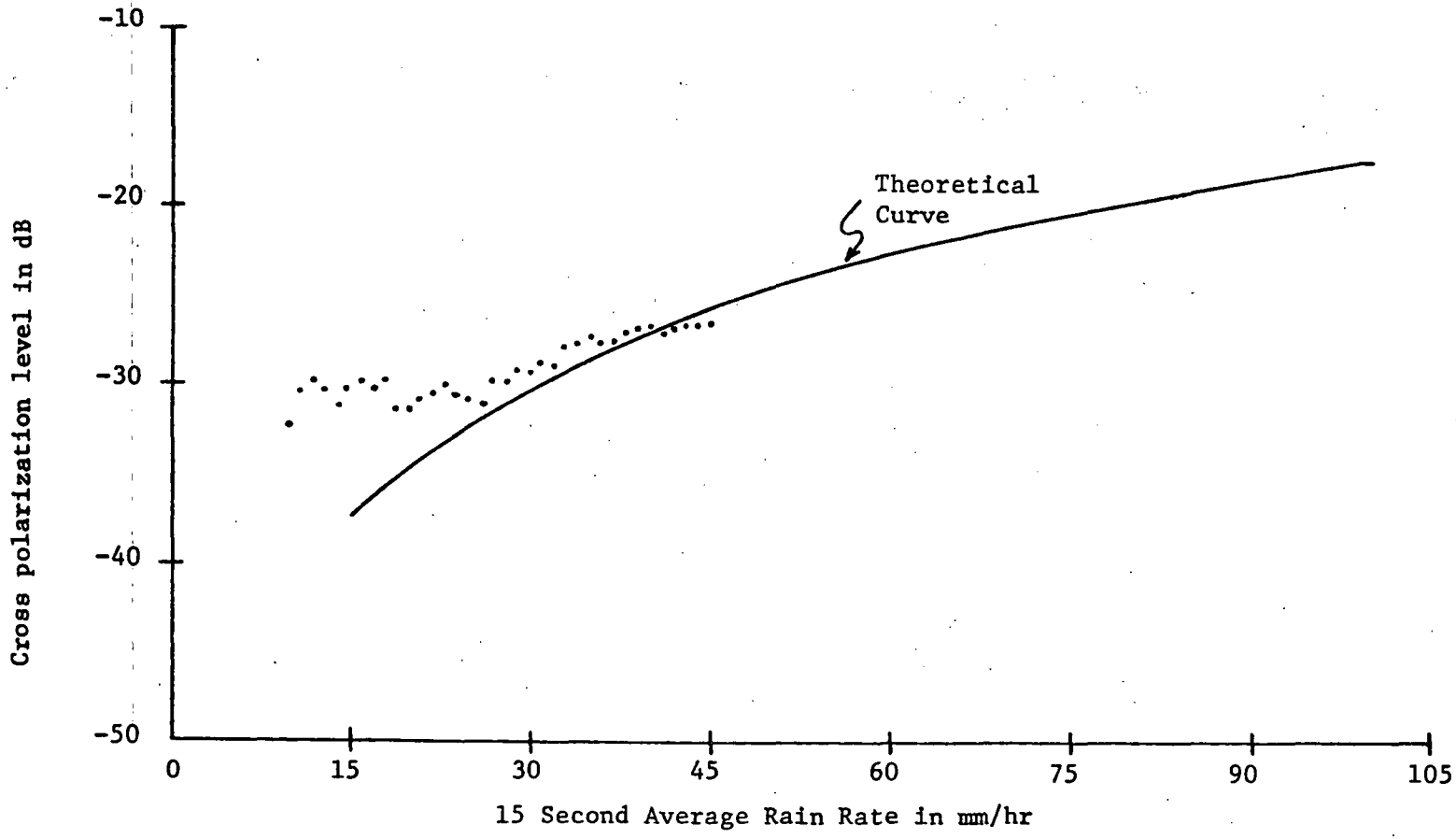


Figure 4.2-3. Average Cross Polarization Level for September 29, 1972.

20 mm/hr. This is because the residual cross polarization level of the system at that time was about -30 dB. These points do not represent an effect of rainfall along the path. The scatter is greatly reduced in this data since all five rain gauges were in operation by this time. The standard deviation is 6-8 dB.

Figure 4.2-4 shows data taken on October 27, 1972. There is good agreement with theory and a lack of scatter which again may be attributed to the operation of all five rain gauges. Standard deviations were not computed for these points.

Figure 4.2-5 presents the average cross polarization level for the six heaviest storms occurring between August 1 and December 31, 1972. Also shown are theoretical curves for both 40% and 100% oblate raindrops. The number of oblate raindrops assumed is seen to have a decided effect on the predicted cross polarization level. Previous to the present work, it has been assumed when computing depolarization that 100% of the drops have the same oblate shape, although Jones [29] has found that a real rain consists of drops with a variety of shapes. He found the following distribution of shapes for all sizes (greater than 1.9 mm equivalent spherical diameter) taken together:

| | |
|---|---|
| spherical | 32% |
| oblate | 28% |
| prolate | 18.5% |
| irregular | 21.5% |

All drop shapes except spherical could contribute to the cross polarization level. About one-half of the prolate drops would be expected to be aligned with their elliptical cross section facing the incident

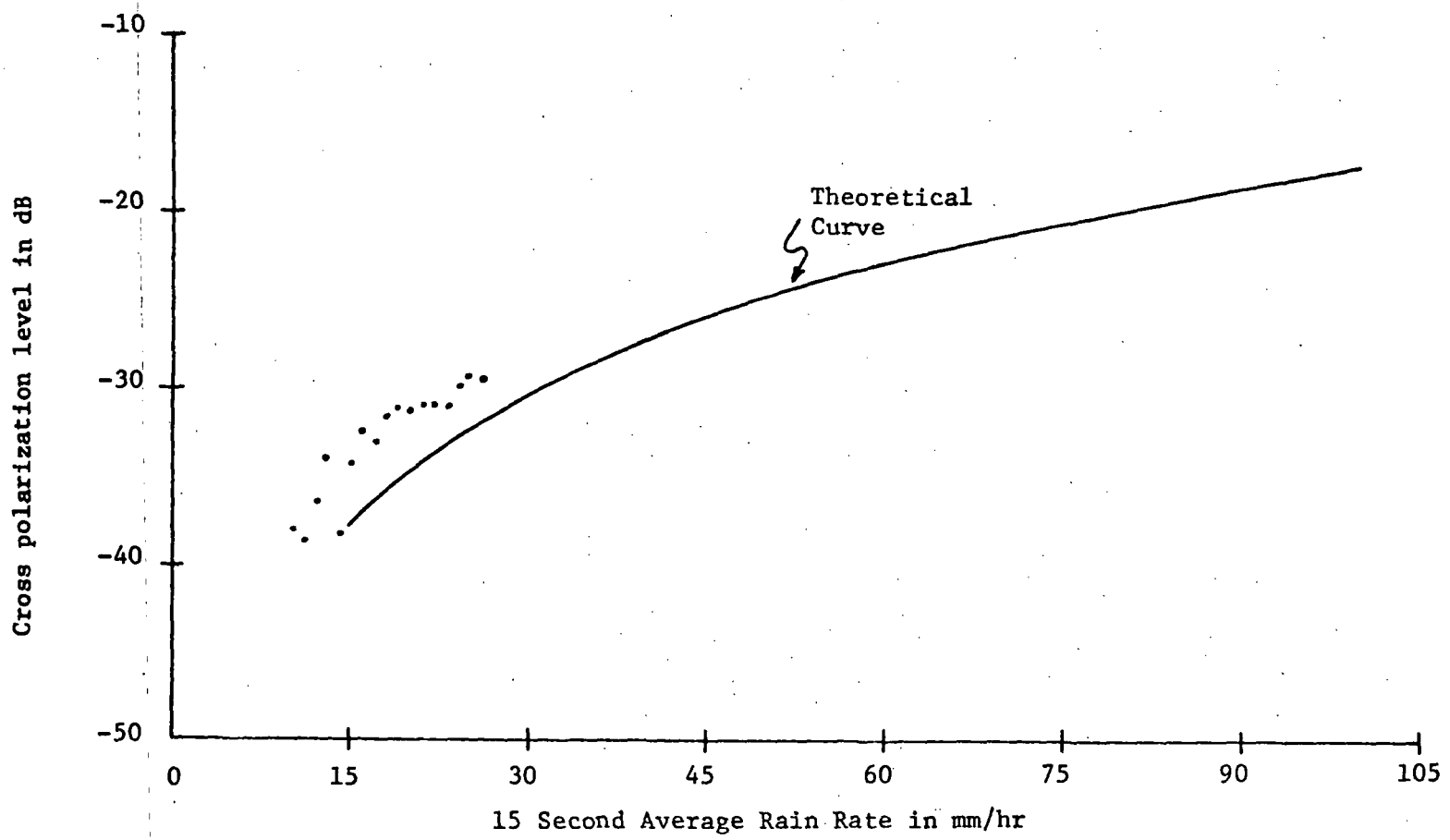


Figure 4.2-4. Average Cross Polarization Level for October 27, 1972.

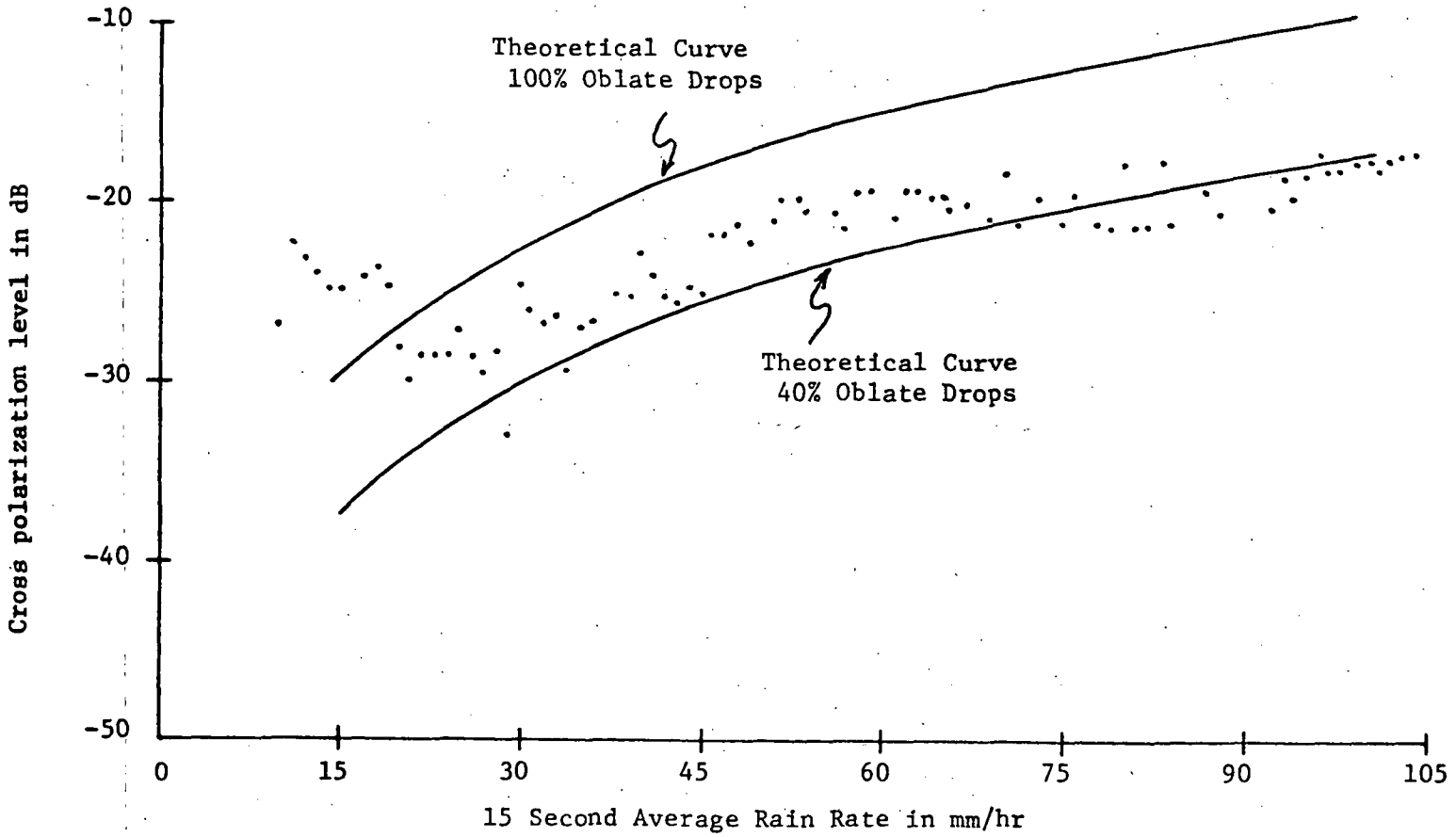


Figure 4.2-5. Average Cross Polarization Level for 6 Storms.

field and therefore produce depolarization. This would increase the effective percentage of oblate drops to about 37%. Since a small but unknown contribution would be made by the irregular drops, the effective percentage of oblate drops was fixed at 40% for this analysis. For percentages near 40% an increase of 5% in the assumed number of oblate drops increases the cross polarization level by about 1 dB for all rain-rates. From Figure 4.2-5, it is evident that an assumption of 40% oblate drops provides good correlation between the theoretical model and the experimental observations.

Another way to compare the theory with the experimental data is to plot attenuation versus rain rate and this is done in Figure 4.2-6 for the storm of August 17. This figure contains the same type of scatter as the figures illustrating the cross polarization levels although the theoretical curve represents the body of the data very well. This scatter is due to an inaccurate determination of the rain rate (due to nonuniform rain along the path) and can be shown by plotting attenuation versus cross polarization thereby eliminating rain rate as a parameter. The result (for the storm of August 17) is shown in Figure 4.2-7 where the scatter is no longer present and an excellent agreement is obtained between theoretical prediction and experimental observation.

From the various figures which have been presented here, it is clear that the new theoretical model of rain depolarization developed in this thesis accurately predicts the average cross polarization and attenuation levels which were observed in the VPI&SU depolarization experiment. In Section 5 a comparison is made with other theoretical and experimental results.

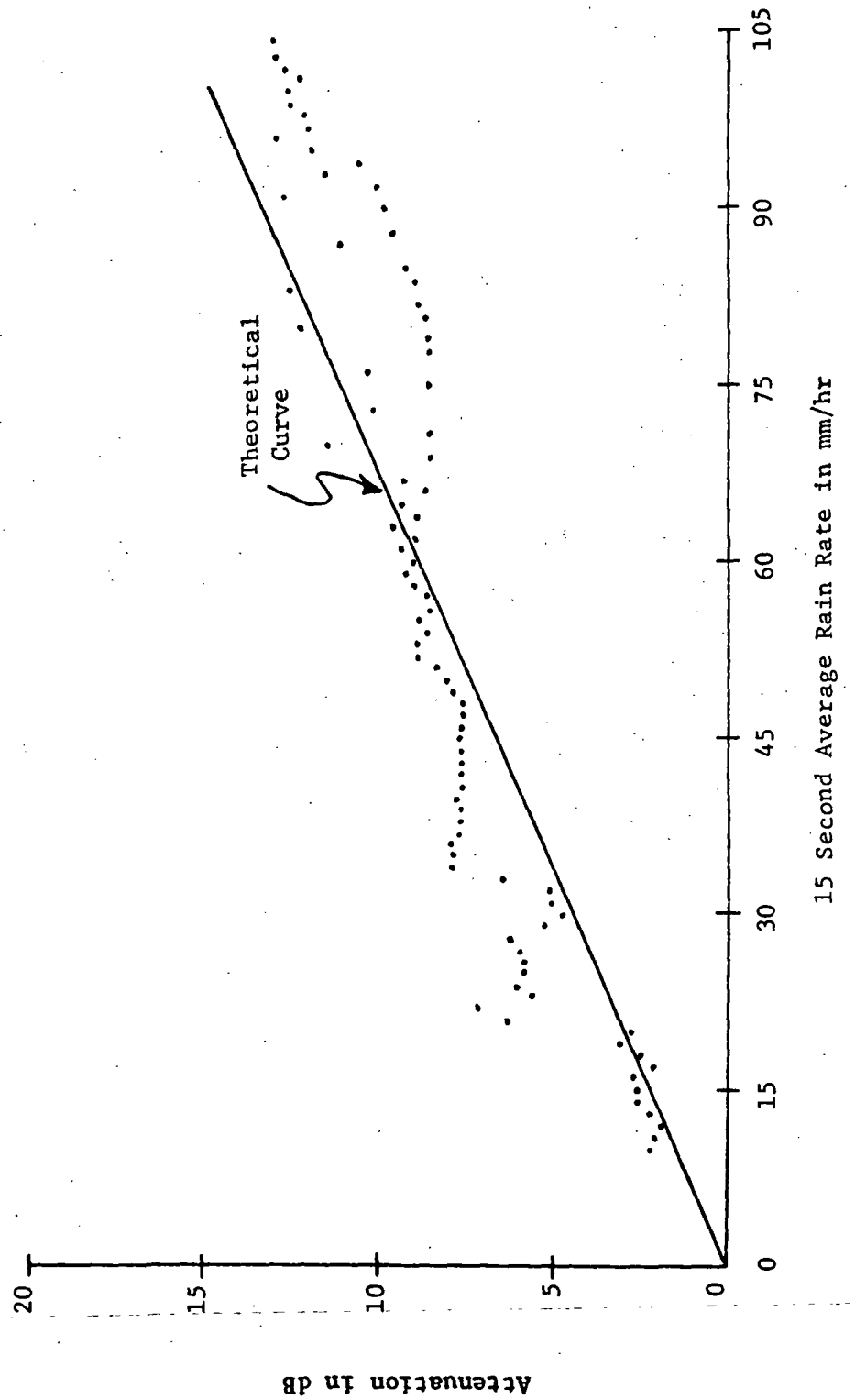


Figure 4.2-6. Average Path Attenuation for August 17, 1972.

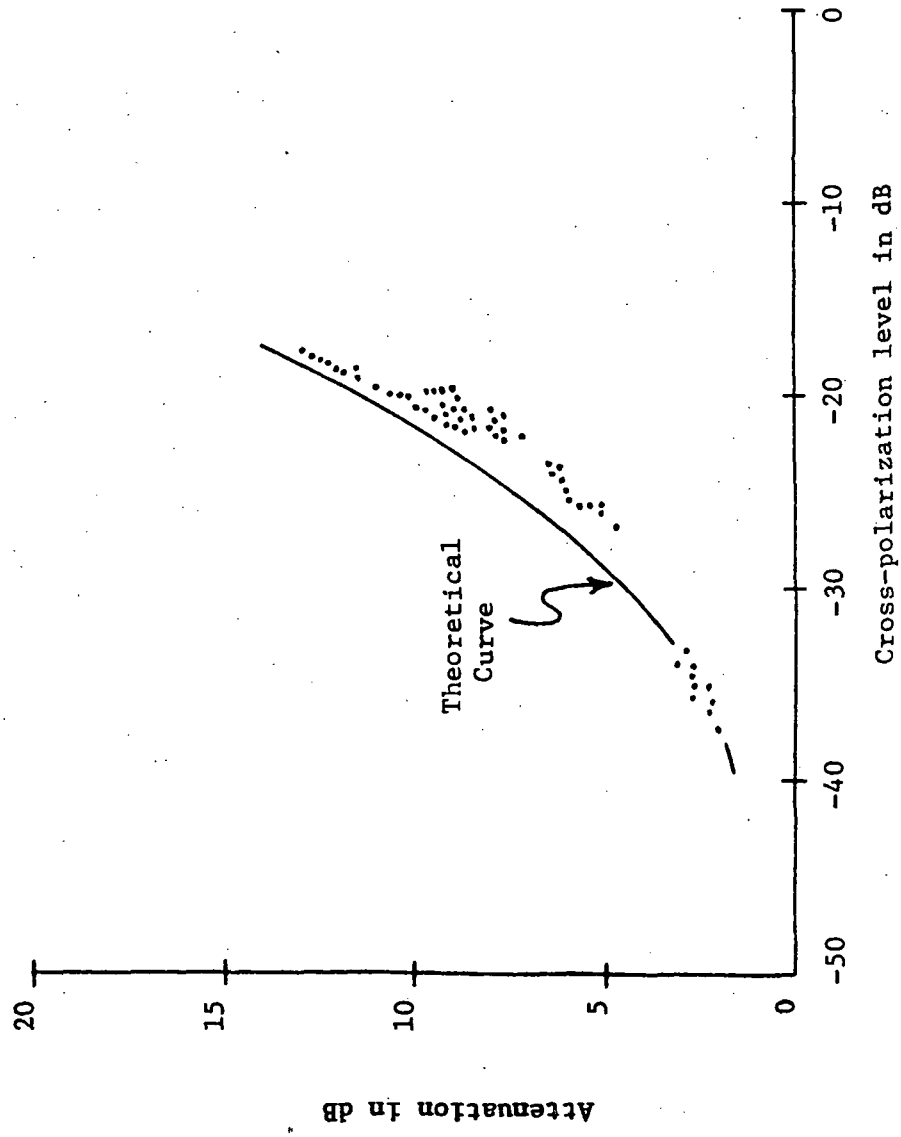


Figure 4.2-7. Average Attenuation Versus Cross Polarization Level for August 17, 1972.

## SECTION V

## RESULTS AND CONCLUSIONS

### 5.1 Comparison with Previous Theories

This thesis has demonstrated that the method of Fresnel zone analysis can be applied with good results to the problem of predicting the cross polarization level during rainfall. Since this approach differs fundamentally from that taken by previous investigators, it provides, for the first time, a theoretical means for checking their results. The most noted work to date is by Oguchi [26] who has calculated attenuation and phase rotation for both vertically and horizontally polarized waves as a function of rain rate. A comparison with his predicted attenuation at 19.3 GHz for a 1.43 km path as a function of rain rate is shown in Figure 5.1-1. As can be seen, the maximum difference between the two curves is about 0.5 dB at 150 mm/hr. Figure 5.1-2 compares Oguchi's computed phase rotations at 19.3 GHz for a 1.43 km path and vertical polarization with those obtained using the new model. The agreement here is not so good as in Figure 5.1-1 but there is as yet no experimental data to support either curve. Another theory which can be checked in light of the present work is the differential attenuation model of depolarization. This method was developed by Thomas [11] and until now was the only way in which the cross polarization level during rainfall could be predicted. A comparison with the differential attenuation prediction using Oguchi's values of attenuation is shown in Figure 5.1-3. For the new model, curves are

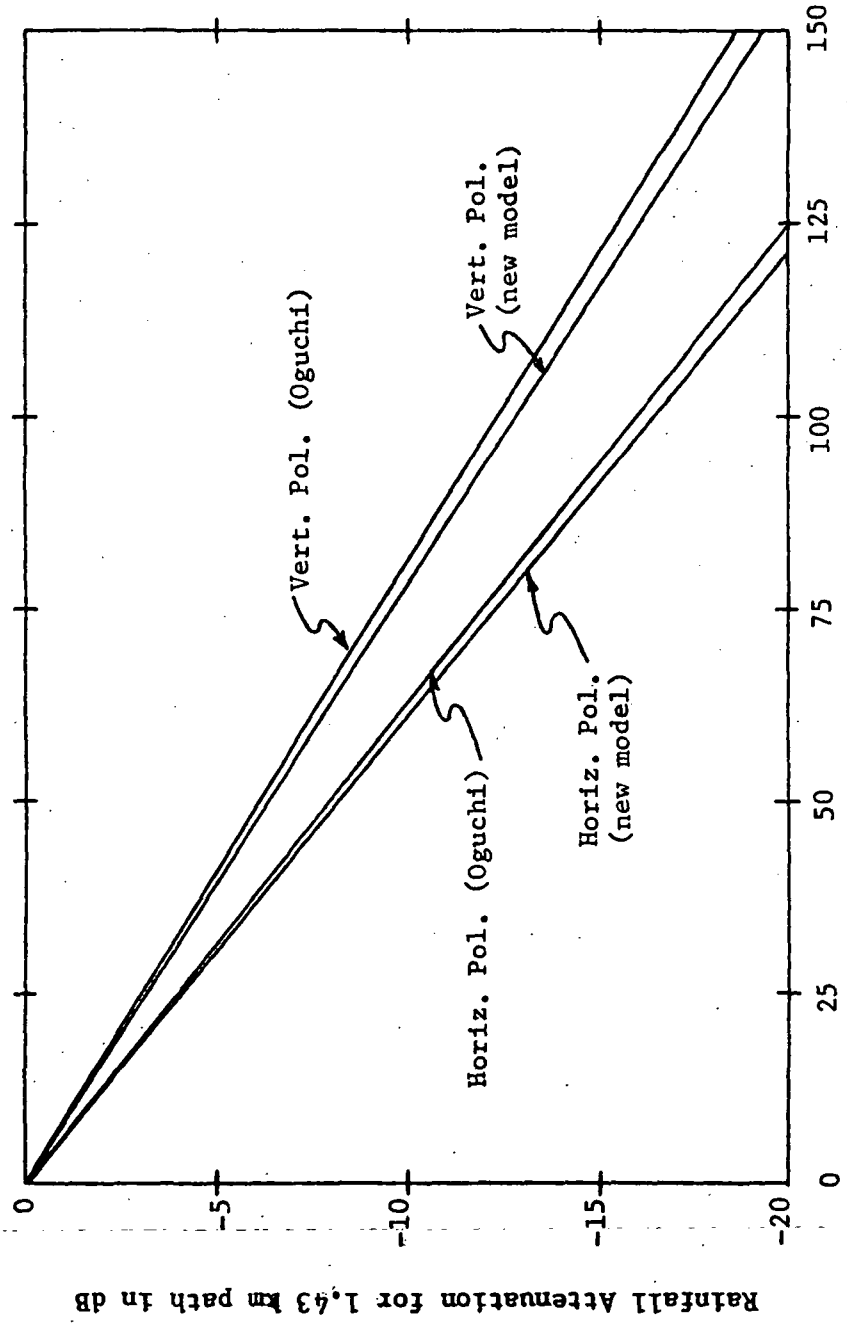


Figure 5.1-1. Theoretical Prediction of Rainfall Attenuation at 19.3 GHz.

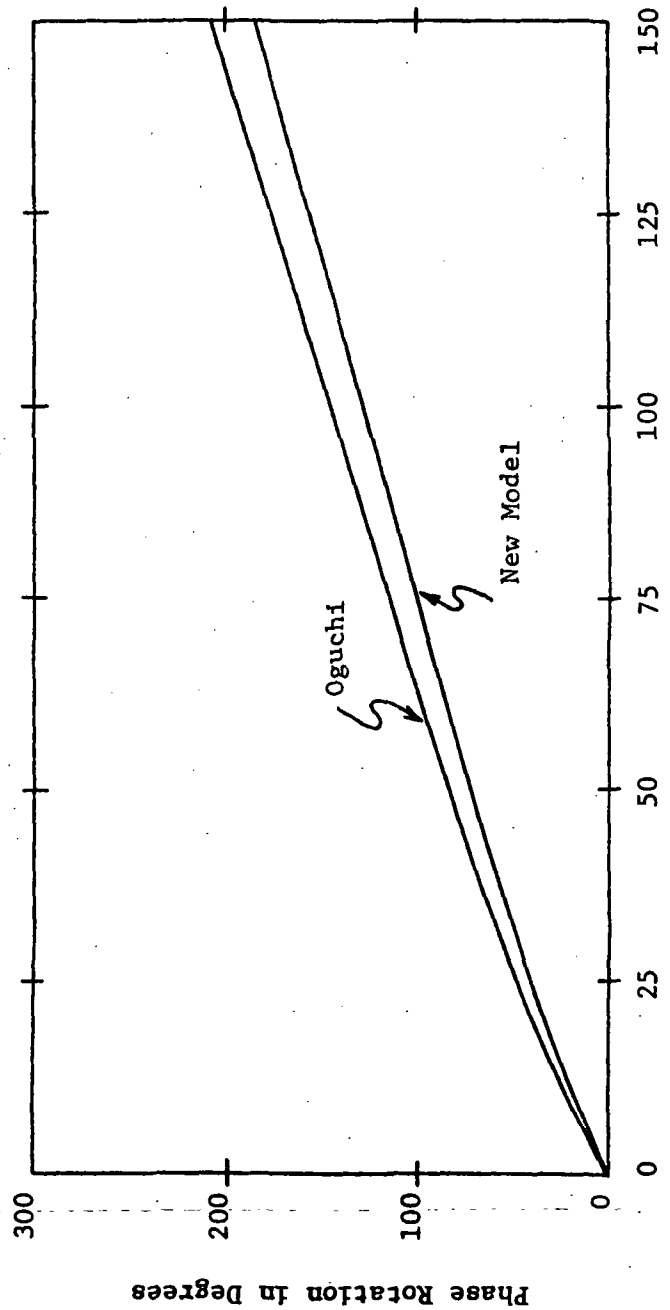


Figure 5.1-2. Theoretical Phase Rotation for Vertical Polarization at 19.3 GHz.

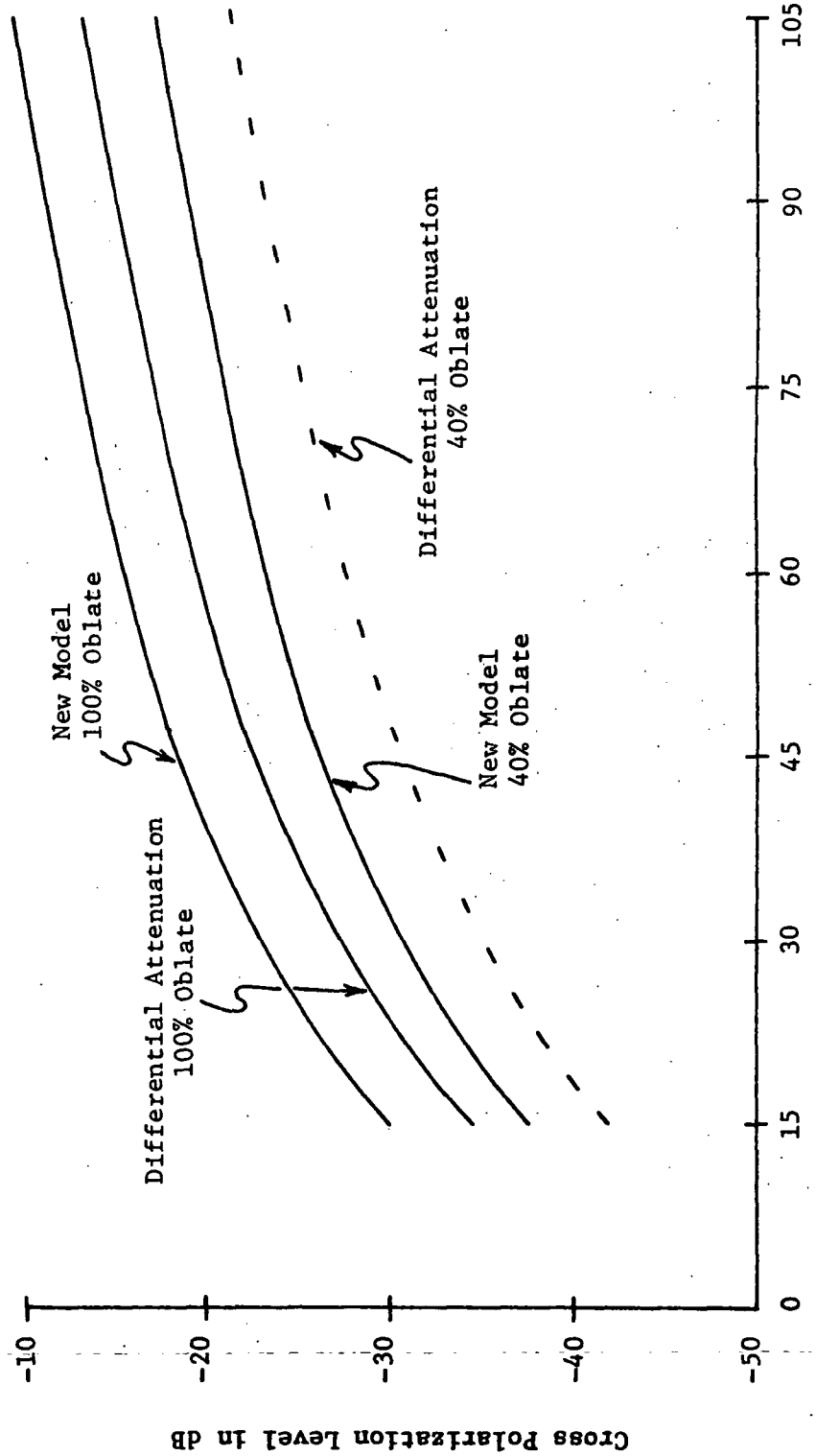


Figure 5.1-3. Theoretical Predictions of the Cross Polarization Level for $\pm 45°$ Polarization on a 1.43 km path at 19.3 GHz.

shown for both 40% and 100% oblate raindrops. As discussed in Section 4.2, the actual effective percentage of oblate drops is near 40% and this is the value which should be used in computations. The 40% curve for the new model is in good agreement with experimental data. However, when using the differential attenuation method, 100% oblate drops is assumed and the middle solid curve of Figure 5.1-3 is obtained. This curve agrees reasonably well with experiment, predicting values that are only slightly high. But the difference in the predicted cross polarization level when assuming 40% and 100% oblate drops is about 8 dB. If the differential attenuation curve is shifted down 8 dB, the dashed curve of Figure 5.1-3 results which is well below experimental observation. Hence, it is concluded that the differential attenuation model of depolarization does not agree well with experimental measurements if a realistic percentage of oblate drops is assumed.

Another conclusion which can be drawn is that the use of a distribution of raindrop sizes is unnecessary in order to get good agreement between theory and experiment. A far more important factor that must be considered (which has been neglected previously) is the effective percentage of oblate raindrops.

## 5.2 Depolarization of Arbitrarily Polarized Waves

The new model of depolarization developed in this thesis may be coupled with the general theory of depolarization of Beckmann [30] to obtain the depolarization by rain of an arbitrary elliptically polarized wave. Beckmann's theory states that the depolarization of an arbitrarily polarized wave can be found if the depolarization of two orthogonal

linearly polarized waves is known. His method is illustrated in Figure 5.2-1 where $\bar{E}_T$ represents the electric field vector of a transmitted arbitrarily polarized wave at a particular instant of time. $\bar{E}_T$ can be resolved into components $\bar{E}_{Tx}$ and $\bar{E}_{Ty}$ along the x and y axes respectively. As $\bar{E}_{Tx}$ propagates toward the receiver, a part of its energy will be converted to a y-polarized wave which is called $\bar{E}_{Rxy}$. The remainder of the energy of $\bar{E}_{Tx}$ which reaches the receiver will still be x-polarized and is denoted by $\bar{E}_{Rxx}$. Similarly, $\bar{E}_{Ty}$ produces a cross polarized component $\bar{E}_{Ryx}$ and a direct component $\bar{E}_{Ryy}$. Hence each component of the received wave is composed of the sum of a direct wave and a cross polarized wave. In equation form,

$$\bar{E}_{Rx} = \bar{E}_{Rxx} + \bar{E}_{Ryx}$$

$$\text{and} \quad \bar{E}_{Ry} = \bar{E}_{Ryy} + \bar{E}_{Ryx}$$

The following depolarization coefficients are defined:

$$\Gamma_{xx} = \frac{\bar{E}_{Rxx}}{\bar{E}_{Tx}} = \frac{\bar{E}_{Rx}}{\bar{E}_{Tx}} \quad \text{when } \bar{E}_{Ty} = 0$$

$$\Gamma_{xy} = \frac{\bar{E}_{Rxy}}{\bar{E}_{Tx}} = \frac{\bar{E}_{Ry}}{\bar{E}_{Tx}} \quad \text{when } \bar{E}_{Ty} = 0$$

$$\Gamma_{yx} = \frac{\bar{E}_{Ryx}}{\bar{E}_{Ty}} = \frac{\bar{E}_{Rx}}{\bar{E}_{Ty}} \quad \text{when } \bar{E}_{Tx} = 0$$

$$\Gamma_{yy} = \frac{\bar{E}_{Ryy}}{\bar{E}_{Ty}} = \frac{\bar{E}_{Ry}}{\bar{E}_{Ty}} \quad \text{when } \bar{E}_{Tx} = 0$$

The $\Gamma$'s are complex quantities and require that both the magnitudes and phases of the received signals be known. The new model provides the

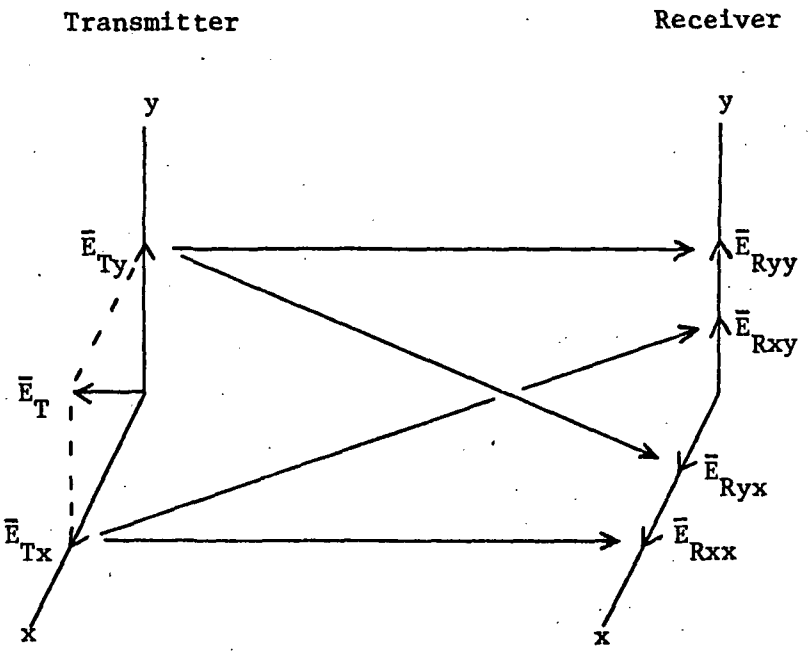


Figure 5.2-1. Expressing depolarization of an arbitrary wave as the sum of the depolarizations of two orthogonal linearly polarized waves.

magnitude and phase for both the direct and the cross polarized wave and allows a computation of Beckmann's depolarization coefficients for a wave propagating through rain. Beckmann shows that

$$P_2 = \frac{\Gamma_{yy} P_1 + \Gamma_{yx}}{\Gamma_{xx} + \Gamma_{xy} P_1}$$

where $P_1$ and $P_2$ are the complex polarization factors of the transmitted and received waves respectively. The received polarization during rain for any transmitted polarization can be computed using the above equation and $\Gamma$'s calculated for the new model.

## 5.3 Preferred Polarization for Depolarization Measurements

Vertical and/or horizontal polarizations have been the choices of most experimenters measuring depolarization by rain. At first thought, this seems to be the logical choice, but it leads to serious problems when it is desired to correlate the experimental data with a theoretical model. The reason is the uncertainty as to the canting angle of the raindrops. The canting angle is the angle which the minor axis of an oblate raindrop makes with the vertical and is zero if the rain is falling straight down. But rain usually does not fall straight down and typical canting angles are in the range from -15° to +15°. Figure 5.3-1 shows the cross polarization level for two paths as a function of the tilt angle, where the tilt angle is defined as the angle between the incident $\bar{E}$ field vector and the minor axis of an oblate raindrop. The cross polarization level for tilt angles of 0° or 90° is $-\infty$. If the transmitted field is polarized either vertically or horizontally, then the canting angle is equal to the tilt angle and a rain with zero canting

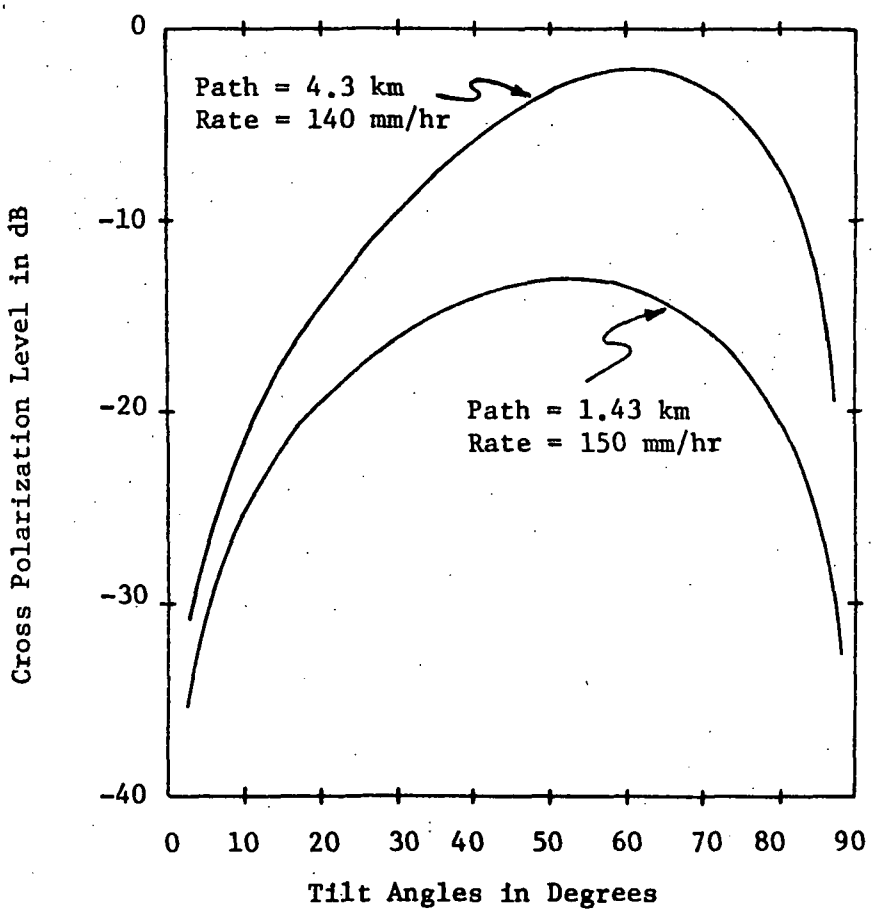


Figure 5.3-1. Variation of Cross Polarization with Tilt Angle at 19.3 GHz.

angle will produce no depolarization (since the cross polarization level is $-\infty$). However, small variations in the canting angle about 0° or 90° produce large changes in the predicted cross polarization level. Since the magnitude of the canting angle could be anywhere from 0° to 15° or more, all that can be done when vertical or horizontal polarization is used is to place broad limits on the expected cross polarization (with $-\infty$ being the lower limit).

In contrast, the curves of Figure 5.3-1 are relatively flat for tilt angles of 45° to 60°. Consider the lower curve which is for the 1.43 km path used in the VPI&SU depolarization experiment. If a transmitted field polarized at 45° from the vertical is assumed, then the tilt angle is 45° when the canting angle is zero. For canting angles of $\pm$15° the tilt angle will range from 30° to 60°. The predicted cross polarization level ranges from a maximum of -13 dB at 55° to a minimum of -16 dB at 30°. The variation is only 3 dB for the expected range of canting angles. The advantage of using $\pm$45° polarization is evident after a comparison of Figure 2.2-5 on page 22 to Figure 4.2-7 on page 50. The former shows the attenuation and cross polarization data that Watson has taken using vertical and horizontal polarization. As can be seen, there is no correlation between theory and experiment. The latter shows data from the VPI&SU depolarization experiment using $\pm$45° polarization. Excellent correlation is obtained in this case.

It is apparent that vertical and horizontal polarization are the poorest choices for a depolarization experiment while $\pm$45° polarization is the best choice when dual channel measurements are to be made.

## 5.4 Polarization Diversity and Frequency Reuse

It is the intent of this section to answer the questions relating to polarization effects which were posed in the Introduction. First, a polarization does exist for which the average attenuation during rainfall is a minimum. Figure 5.4-1 shows the attenuation on a 1.43 km path at 19.3 GHz as a function of tilt angle. If it is assumed that positive and negative canting angles are equally likely then the time average canting angle is zero and the average tilt angle is equal to the polarization angle of the transmitted field. Then 0° and 90° tilt angles represent vertical and horizontal polarization respectively. From Figure 5.4-1, the attenuation is minimum for a tilt angle of 0°. Therefore, on the average, vertical polarization will suffer the least attenuation.

What two orthogonal polarizations exhibit the least cross polarization interference? This question can be answered with reference to Figure 5.3-1 and with the assumption that the magnitude of the canting angle is about 15°. For a short path such as illustrated by the lower curve, vertical and horizontal polarizations produce the least cross polarization interference. For a canting angle of 15° the tilt angle for vertical polarization is 15° and the cross polarization level is -22 dB. The tilt angle for horizontal polarization is 90° - 15° or 75° and the corresponding level is -17 dB. For a 45° tilt angle the cross polarization level is about -13 dB. Clearly, horizontal and vertical polarization produce the least mutual interference for a 1.43 km path. However, this advantage decreases as the path length increases. For

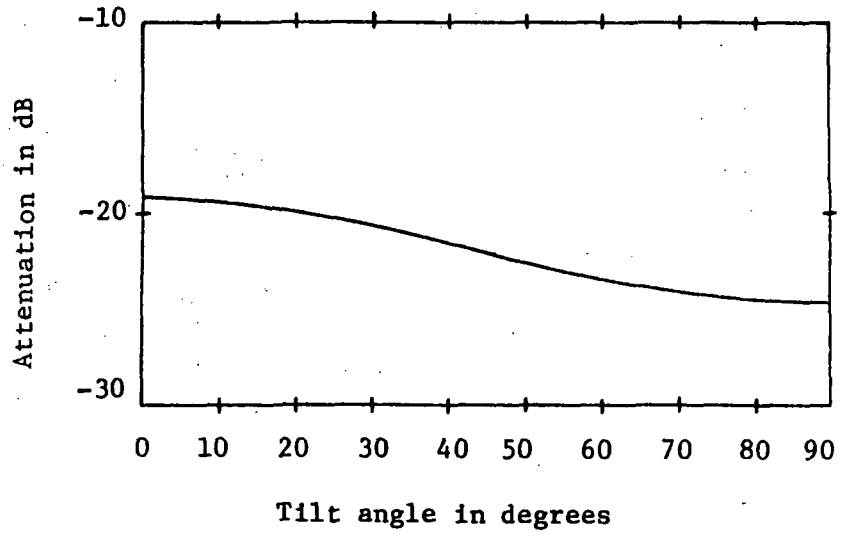


Figure 5.4-1. Attenuation for a Rain Rate of 150 mm/hr, a Path Length of 1.43, and a Frequency of 19.3 GHz.

longer paths, such as illustrated by the upper curve in Figure 5.3-1, the peak of the cross polarization versus tilt angle curve shifts toward horizontal polarization (90° tilt angle). This means that the cross polarization level for horizontal polarization is increasing more for a given increase in path length than is the level for other polarizations. This effect quickly eliminates the advantage of using vertical and horizontal polarization (at the same frequency) as two separate communications channels.

This shift of the peak toward horizontal polarization is supported by Shimba [31] who made measurements of cross polarization interference using horizontal polarization at a frequency of 19.1 GHz. He observed a cross polarization level of -10 dB with a rain rate of 140 mm/hr on a 4.3 km path. Referring to the top curve in Figure 5.3-1, this implies a canting angle of about 8° since a -10 dB cross polarization level occurs for a tilt angle of 82°. A canting angle of 8° is within the expected range.

The question of how long a path can be if polarization multiplexing is to be used is answered in the next two figures for the two polarization configurations discussed here. Figure 5.4-2 shows the cross polarization level as a function of path length for a tilt angle of 60°. A tilt angle of 60° is the worst case condition for a $\pm$45° polarization multiplexed system and represents the 45° $\bar{E}$ field polarization plus a 15° canting angle. If a maximum acceptable cross polarization level of -10 dB is assumed, then the maximum path length is 7 km for a 50 mm/hr rain rate. However, for a rain rate of 100 mm/hr

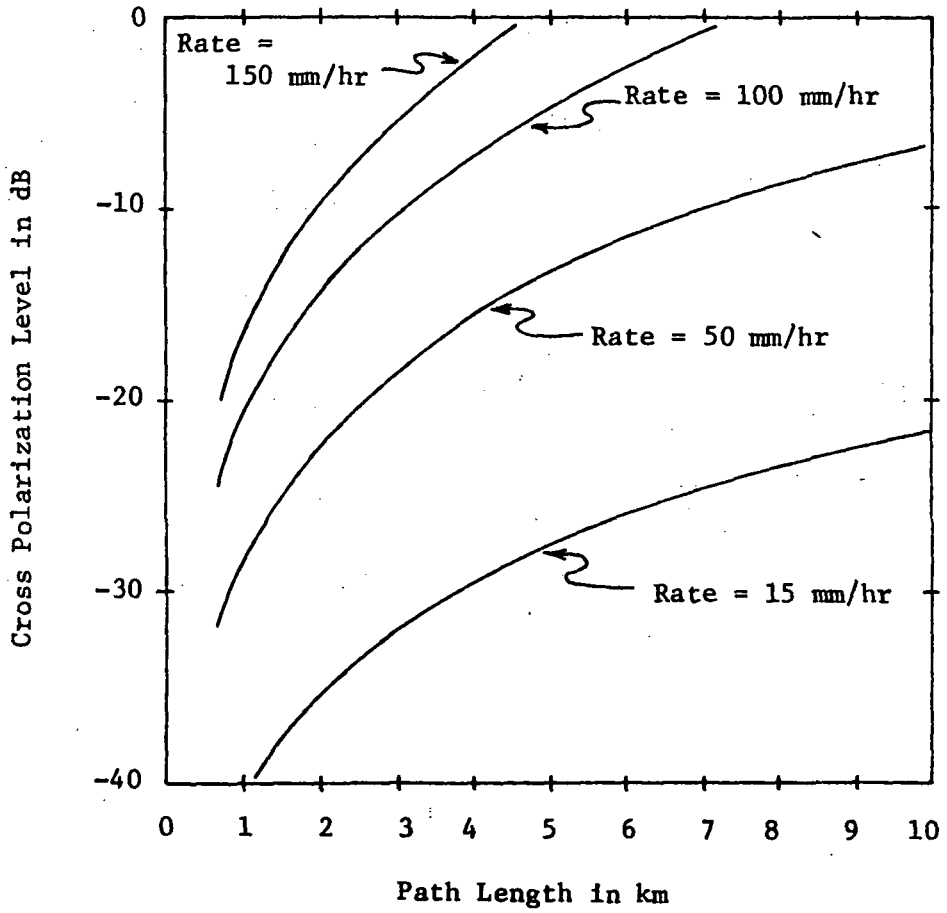


Figure 5.4-2. Cross Polarization vs. Path Length for a Tilt Angle of 60° and a Frequency of 19.3 GHz.

the maximum path length is reduced to 3 km and for 150 mm/hr it is only 2 km.

Figure 5.4-3 shows the cross polarization level versus path length for a tilt angle of 75°. This tilt angle is the worst case condition when a multiplexed system using vertical and horizontal polarization is employed and represents the 90° horizontal polarization minus a 15° canting angle. With the same -10 dB maximum acceptable cross polarization level, the maximum path lengths corresponding to rain rates of 50, 100, and 150 mm/hr are 11, 4.5, and 2.8 km respectively. Since rain rates of 150 mm/hr are not uncommon in many parts of the United States, the maximum path length would be limited to 2 km if ±45° polarization multiplexing is to be employed and to 2.8 km if vertical and horizontal polarizations are used.

The question as to the feasibility of using two polarizations which do not fade simultaneously to increase the reliability of a communications system is important from a practical standpoint. To answer this question one must realize that a system designed to minimize attenuation would of necessity employ vertical or near-vertical polarization since the attenuation is minimum for a tilt angle of 0°. For a constant rain rate the attenuation would vary as the canting angle varied from 0° to about 15°. From Figure 5.4-1 the difference in attenuation between a tilt angle of 0° and one of 15° is about 0.3 dB for the 1.43 km path or about 0.2 dB/km. Assuming vertical polarization, the minimum attenuation would occur for a canting angle of 0° and would be expected to increase by about 0.2 dB/km when the canting angle increased to 15°. For a 10 km path this represents an increase of, at most, 2 dB

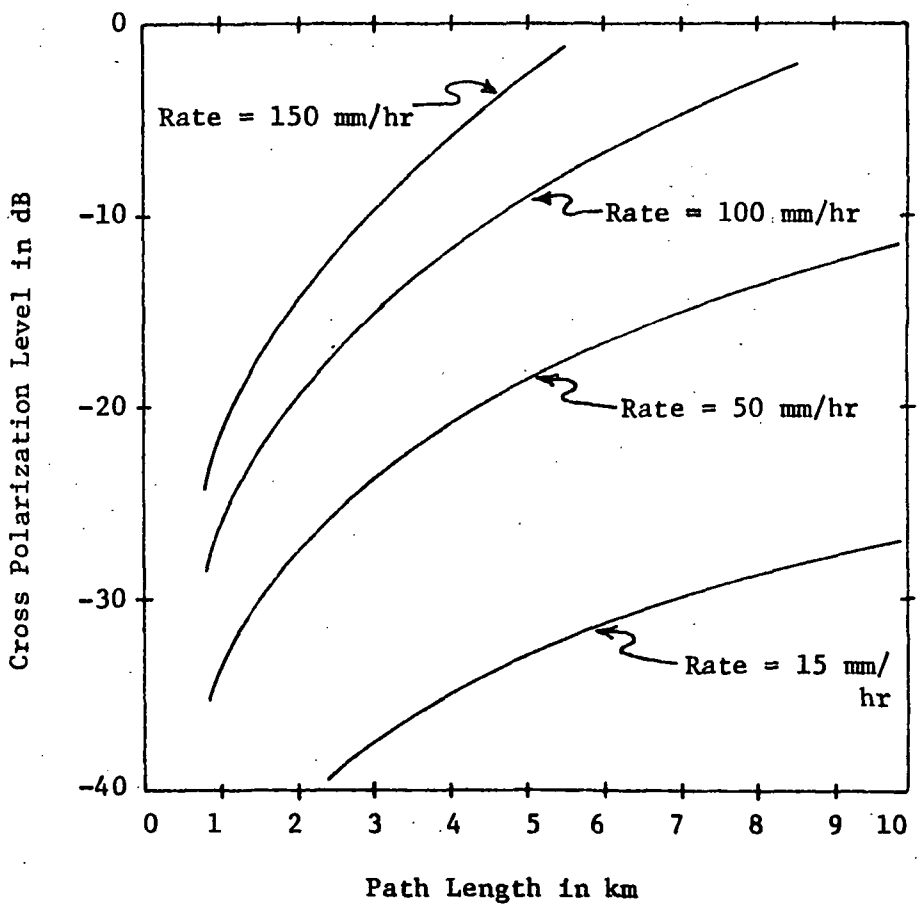


Figure 5.4-3. Cross Polarization vs. Path Length for a Tilt Angle of 75° and a Frequency of 19.3 GHz.

above the minimum attenuation level. Hence, all that could be gained by employing another channel is 2 dB less attenuation for a 10 km path. This would indicate that polarization diversity is not feasible as a means of increasing resistance to fading in a communications system.

## SUMMARY

Weather--especially precipitation--is a major consideration in the design of millimeter wave communications systems. The two major effects of weather are attenuation and depolarization of a transmitted wave due to rainfall. Most theoretical and experimental work to date has been concerned with the attenuation produced by rain while the depolarization effects have been comparatively ignored. The only theoretical model of depolarization prior to this work was the differential attenuation model proposed by Thomas. A few investigators had measured cross polarization levels during rain, but limitations inherent in their methods made an accurate comparison with theory virtually impossible. Hence, not only a new model of depolarization by rainfall was needed, but also a new experiment conducted under conditions which would allow an accurate check of the theory.

The work reported here satisfies both of these needs. A new theoretical model was developed based on the summation of the scattered fields from an ensemble of rain drops. The model forms the basis of a computer program which was written to calculate the expected attenuation and cross polarization levels during rainfall. Simultaneously, an experiment was begun at Virginia Polytechnic Institute and State University to measure the effects of rain on millimeter waves. Data from this experiment are presented here and excellent agreement is shown between the data and calculations based on the new model.

Computations based on the new theory of depolarization developed

in this thesis allow several conclusions to be drawn regarding the influence of polarization on millimeter wave propagation through rain. The conclusions are: (1) the best polarizations to use for a depolarization experiment are $\pm 45°$ from the vertical, (2) vertical and horizontal polarizations should not be used for a depolarization experiment, (3) vertical polarization suffers the least average attenuation during rainfall, (4) Oguchi's attenuations and phase rotations for 19.3 GHz are correct, (5) the effective percentage of oblate drops assumed in an analysis is critical to the predicted cross polarization level, (6) polarization diversity is not feasible as a means of increasing resistance to rain-induced fading, and (7) the use of polarization multiplexing utilizing orthogonal polarizations is limited to very short path lengths.

## LITERATURE CITED


[1] Mie, G., "Beitrüge zur Optik trüber Medien, speziell kolloidaler Metallosungen," Ann. der Phys., Vol. 25, Mar 1908, pp. 377-445.

[2] Ryde, J. W., and D. Ryde, "Attenuation of Centimetre Waves by Rain, Hail and Clouds," Rept 8516, General Electric Co. Research Labs., Wembley, England, Aug 1944.

[3] _____, "Attenuation of Centimetre and Millimetre Waves by Rain, Hail, Fogs and Clouds," Rept 8670, General Electric Co. Research Labs., Wembley, England, May 1945.

[4] Medhurst, R. G., "Rainfall Attenuation of Centimeter Waves: Comparison of Theory and Measurement," IEEE Trans. on Antennas and Propagation, Vol. 13, No. 4, July 1965, pp. 550-564.

[5] Oguchi, T., "Attenuation of Electromagnetic Waves Due to Rain with Distorted Raindrops," J. Radio Res. Lab., Jap., Vol. 7, 1960, pp. 467-485.

[6] _____, "Attenuation of Electromagnetic Waves Due to Rain with Distorted Drops," J. Radio Res. Lab., Jap., Vol. 11, 1964, pp. 19-44.

[7] Laws, J. O., and D. A. Parsons, "The Relation of Raindrop-size to Intensity," Trans. Am. Geophysical Union, Vol. 24, 1943, pp. 432-460.

[8] Best, A. C., "Empirical Formulae for the Terminal Velocity of Water Drops Falling Through the Atmosphere," Quart. J. R. Met. Soc., Vol. 76, July 1950, pp. 302-311.

[9] van de Hulst, H. C., Light Scattering by Small Particles, New York: John Wiley Sons, Inc., 1957, pp. 28-34.

[10] Setzer, D. E., "Computed Transmission Through Rain at Microwave and Visible Frequencies," B.S.T.J., Vol. 49, No. 8, Oct. 1970, pp. 1873-1892.

[11] Thomas, D. T., "Cross Polarization Distortion in Microwave Radio Transmission Due to Rain," Radio Science, Vol. 6, No. 10, Oct. 1971, pp. 833-840.

[12] Adam, M. G., R. A. Hull, and C. Hurst, "Absorption of 1 cm Radiation by Rain," Rept C. L. Misc. 3, C. V. D. Research Group, New Clarendon Lab., Oxford, England, Jun 1942.

[13] Hathaway, S. D., and H. W. Evans, "Radio Attenuation at 11 kmc and Implications Affecting Relay System Engineering," B.S.T.J., Vol. 38, Jan 1959, pp. 73-98.

[14] Rado, G. T., "Measurements of the Attenuation of K-band Waves by Rain," Rept 603, Radiation Lab., M.I.T., Cambridge, Mar 1945.

[15] Okamura, S., K. Funakawa, H. Uda, J. Kato, and T. Oguchi, "On the Measurement of Attenuation by Rain at 8.6 mm Wavelength," J. Radio Research Labs., Jap., Vol. 6, Apr 1959, pp. 255-267.

[16] _____, "Effect of Polarization on the Attenuation by Rain at Millimeter Wavelength," J. Radio Research Labs., Jap., Vol. 8, Mar 1961, pp. 73-80.

[17] Funakawa, K., and J. Kato, "Experimental Studies of Propagation Characters of 8.6 mm Waves on the 24 km Path," J. Radio Research Labs., Jap., Vol. 9, Sep 1962, pp. 351-367.

[18] Anderson, L. J., J. P. Day, C. H. Freres, and A. P. D. Stokes, "Attenuation of 1.25-centimeter Radiation Through Rain," Proc. IRE, Vol. 35, Apr 1947, pp. 351-354.

[19] Semplak, R. A., and R. H. Turrin, "Some Measurements of Attenuation by Rainfall at 18.5 GHz," B.S.T.J., Vol. 48, Jul-Aug 1969, pp. 1767-1787.

[20] Semplak, R. A., "Effect of Oblate Raindrops on Attenuation at 30.9 GHz," Radio Science, Vol. 5, No. 3, Mar 1970, pp. 559-564.

[21] _____, "Dual Frequency Measurements of Rain-induced Microwave Attenuation on a 2.6-kilometer Propagation Path," B.S.T.J., Vol. 50, No. 8, Oct 1971, pp.2599-2605.

[22] Skerjanec, R. E., and C. A. Samson, "Rain Attenuation Measurements in Mississippi at 10 and 14.43 GHz," IEEE Trans. on Antennas and Propagation, Vol. 19, Jul 1971, pp. 575-577.

[23] Watson, P. A., "Measurements of Linear Cross-Polarization at 11 GHz," Report to European Space Research Organization, Contract No. 1297/SL, U. of Bradford, Bradford, England, May 1972.

[24] Semplak, R. A., and H. E. Keller, "A Dense Network for Rapid Measurement of Rainfall Rate," B.S.T.J., Vol. 48, Jul-Aug 1969, pp. 1745-1756.

[25] Livingston, D. C., The Physics of Microwave Propagation, Englewood Cliffs, New Jersey: Prentice-Hall, 1970, pp.19-56.

[26] Oguchi, T., "Attenuation and Phase Rotation of Radio Waves Due to Rain: Calculations at 19.3 and 34.8 GHz," Radio Science, Vol. 8, No. 1, Jan 1973.

[27] Bostian, C. W., and W. L. Stutzman, "The Influence of Polarization on Millimeter Wave Propagation Through Rain," Semi-annual Status Report I, NASA Grant NGR-47-004-091, VPI&SU, Blacksburg, Jul 1972.

[28] Bostian, C. W., and W. L. Stutzman, "The Influence of Polarization on Millimeter Wave Propagation Through Rain," Semi-annual Status Report II, NASA Grant NGR-47-004-091, VPI&SU, Blacksburg, Jan 1973.

[29] Jones, D. M. A., "The Shape of Raindrops," Journal of Meteorology, Vol. 16, Oct 1959, pp. 504-510.

[30] Beckmann, P., The Depolarization of Electromagnetic Waves, Boulder, Colorado: The Golem Press, 1968, pp. 39-41.

[31] Shimba, M., and K. Morita, "Radio Propagation Characteristics Due to Rain at 19 GHz," 1972 G-AP International Symposium Digest, Dec 1972, pp. 246-249.

## APPENDIX

## NUMERICAL METHODS

Before the scattering coefficients ($S_{pq}$'s) of Section 3.3.2 can be evaluated, the single drop scattering functions ($f_{pq}$'s) and the imaginary constant K must be determined.

The $f_{pq}$'s are computed using the scattering functions, $f_v$ and $f_h$, which Oguchi has recently published [26]. Assuming zero canting angle for a raindrop, $f_v$ is the ratio of the scattered $\bar{E}$ field from the drop which is vertically polarized to the incident vertically polarized $\bar{E}$ field, and $f_h$ is the ratio of the scattered $\bar{E}$ field from the drop which is horizontally polarized to the incident horizontally polarized $\bar{E}$ field.

With reference to Figure A-1, $\bar{E}^i_1$ is the incident $\bar{E}$ field on the drop which has polarization 1 making an angle $\theta$ with the vertical as shown. $\bar{E}^i_1$ is decomposed into components $\bar{E}^i_v$ and $\bar{E}^i_h$ along the vertical and horizontal axes respectively.

$$\bar{E}^i_v = \bar{E}^i_1 \cos\theta \qquad\qquad \bar{E}^i_h = \bar{E}^i_1 \sin\theta$$

$\bar{E}^i_v$ and $\bar{E}^i_h$ are scattered by the drop producing $\bar{E}^s_v$ and $\bar{E}^s_h$.

$$\bar{E}^s_v = f_v \bar{E}^i_v = f_v \bar{E}^i_1 \cos\theta$$

$$\bar{E}^s_h = f_h \bar{E}^i_h = f_h \bar{E}^i_1 \sin\theta$$

$\bar{E}^s_v$ and $\bar{E}^s_h$ have components $\bar{E}^s_{v_1}$ and $\bar{E}^s_{h_1}$ in the polarization 1 direction which add to give the total scattered field which is 1 polarized.

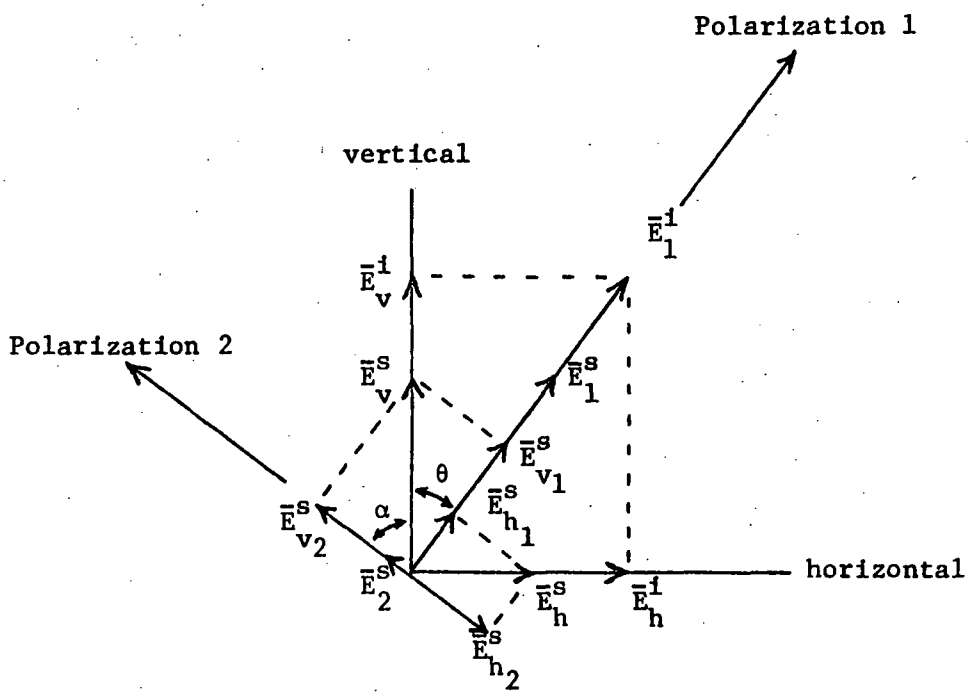


Figure A-1. Geometry for Computing $f_{pq}$.

$$\bar{E}^s_{v_1} = \bar{E}^s_v \cos\theta = f_v \bar{E}^i_1 \cos^2\theta$$

$$\bar{E}^s_{h_1} = \bar{E}^s_h \sin\theta = f_h \bar{E}^i_1 \sin^2\theta$$

$$\bar{E}^s_1 = \bar{E}^s_{v_1} + \bar{E}^s_{h_1} = \bar{E}^i_1 (f_v \cos^2\theta + f_h \sin^2\theta)$$

Then $f_{11}$ is defined as the ratio of $\bar{E}^s_1$ to $\bar{E}^i_1$

$$f_{11} = \frac{\bar{E}^s_1}{\bar{E}^i_1} = f_v \cos^2\theta + f_h \sin^2\theta$$

$\bar{E}^s_v$ and $\bar{E}^s_h$ have components $\bar{E}^s_{v_2}$ and $\bar{E}^s_{h_2}$ in the polarization 2 direction which add to give the total scattered field which is 2 polarized.

$$\bar{E}^s_{v_2} = \bar{E}^s_v \sin\theta = f_v \bar{E}^i_1 \sin\theta\cos\theta$$

$$\bar{E}^s_{h_2} = \bar{E}^s_h \cos\theta = f_h \bar{E}^i_1 \sin\theta\cos\theta$$

$$\bar{E}^s_2 = \bar{E}^s_{v_2} + \bar{E}^s_{h_2} = \bar{E}^i_1 (f_v - f_h) \sin\theta\cos\theta$$

Then $f_{12}$ is defined as the ratio of $\bar{E}^s_2$ to $\bar{E}^i_1$

$$f_{12} = \frac{\bar{E}^s_2}{\bar{E}^i_1} = (f_v - f_h) \sin\theta\cos\theta$$

The coefficient $f_{22}$ is obtained from the expression for $f_{11}$ by replacing $\theta$ with $\alpha$ where

$$\alpha = \theta - 90°$$

Then $f_{22} = \frac{\bar{E}^s_2}{\bar{E}^i_2} = f_v \cos^2\alpha + f_h \sin^2\alpha.$

The determination of the constant K requires an evaluation of the summation

$$\Sigma\, e^{-jkr}$$

which is to be performed over all drops (in the plane at midpath) which are contained in the first Fresnel zone, and where r is the distance from the drop being considered to the receiver. With reference to Figure A-2, point O is the intercept of the line of sight with the plane of drops. Since only the relative phases of the waves from different drops are significant, one may assume that the phase of the wave passing through point O is zero. The summation then becomes

$$\Sigma\ e^{-jk(r - R)2}$$

where the factor of 2 arises because the incident wave on the drop also travels the extra distance (r - R).

$$\text{But } r - R \approx \frac{\rho^2}{2R} = \frac{\rho^2}{L}$$

$$\text{Then } \Sigma\ e^{-jk(r - R)2} \approx \Sigma\ e^{-j2k\,\rho^2/L}$$

If one divides the first Fresnel zone (radius = $F_1$) into M intervals as follows

$$\rho_m = \sqrt{m - 1/2}\ \frac{F_1}{\sqrt{M}} \qquad 0 \leq m \leq M$$

then the phase lag $\psi$ at any point is

$$\psi = -\frac{2k\rho_m^{\,2}}{L} = -\frac{2k}{L}\frac{F_1^{\,2}}{M}(m - 1/2)$$

From Section 3.2,

$$F_1^{\,2} = \frac{\lambda\ell(L-\ell)}{L}$$

$$= \frac{\lambda L/2(L-L/2)}{L} = \lambda/2(L-L/2) \qquad \text{at } \ell = L/2$$

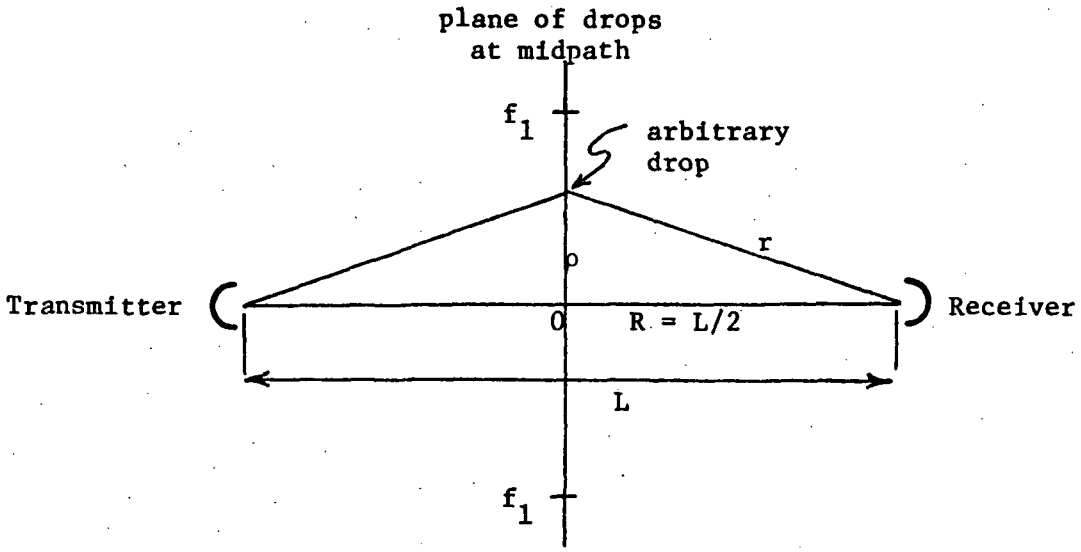


Figure A-2. Geometry for Approximating Phase Lag of Scatter From Arbitrary Drop in the First Fresnel Zone.

$$\text{Then } \psi = -\frac{4\pi}{\lambda L}\frac{\lambda}{2}(L - L/2)\frac{1}{M}(M - 1/2)$$

$$= -\frac{\pi}{M}(M - 1/2)$$

and the phase shift from point $r_m$ to $r_{m+1}$ is constant at $-\frac{\pi}{M}$ radians.

$$\text{Now } \sum_{\substack{\text{all}\\ \text{drops}}} e^{-jk(r - R)2} \simeq \frac{D}{M}\sum_{m=1}^{M} e^{-j\frac{\pi}{M}(m - 1/2)}$$

since there are $\frac{D}{M}$ drops in each interval where D is the total number of drops in the first Fresnel zone.

$$\text{But } \sum_{m=1}^{M} e^{-j\frac{\pi}{M}(m - 1/2)}$$

$$= e^{+j\frac{\pi}{2M}} e^{-j\frac{\pi}{M}} \sum e^{-j\frac{\pi}{M}(m - 1)}$$

$$= e^{-j\frac{\pi}{2M}} \sum_{p=0}^{M-1} e^{-j\frac{\pi}{M}p}$$

$$= e^{-j\frac{\pi}{2M}} \frac{1 - e^{-j\pi}}{1 - e^{-j\frac{\pi}{M}}}$$

$$= e^{-j\frac{\pi}{2M}} \frac{2}{1 - e^{-j\frac{\pi}{M}}}$$

$$= 1 \cdot \frac{2}{-(-j\,\pi/M)} = -j\frac{2}{\pi}M \quad \text{for M large}$$

$$\text{Then } \sum_{\substack{\text{all}\\ \text{drops}}} e^{-jk(r - R)2} \simeq \frac{D}{M}(-j\frac{2}{\pi}M) = -j\frac{2}{\pi}D$$

$$\text{Hence, } K = -j\frac{2}{\pi}$$

The following computer program was written in FORTRAN IV incorporating the method developed in this thesis. The program is followed by a description of the variables and a discussion of convergence.

```
      COMPLEX FV,FH,FM,FX,MINUSJ,FXM,S11,S22,S12,EM,EX,E
      REAL N
      COMPLEX CMPLX
    6 READ(5,1)PATHL,RATE,THETA,N
    1 FORMAT(4F10.0)
      IF(N.EQ.0.)GO TO 5
C     N MUST BE EVEN
      ALPHA=THETA-90.
      THETA=THETA/57.295
      ALPHA=ALPHA/57.295
      P=0.40
      DMODE=1.+0.9*ALOG10(RATE)
      FVR=(0.1503+((DMODE-2.)**1.256)*0.2226)*0.001
      FVI=(-0.06914-((DMODE-2.)**1.294)*0.19946)*0.001
      FHR=(0.1677+((DMODE-2.)**1.306)*0.2986)*0.001
      FHI=(-0.07757-((DMODE-2.)**1.421)*0.2653)*0.001
      FV=CMPLX(FVR,FVI)
      FH=CMPLX(FHR,FHI)
      F11=FV*COS(THETA)*COS(THETA+FH*SIN(THETA)*SIN(THETA)
      F12=(FV-FH)*SIN(THETA)*COS(THETA)
      F22=FV*COS(ALPHA)*COS(ALPHA)+FH*SIN(ALPHA)*SIN(ALPHA)
      R=PATHL/2.
      R1=R-PATHL/(2.*N)
      R2=R+PATHL/(2.*N)
      VOLUME=3.14159*0.0155*((R2*R2/2.-R2*R2*R2/(3.*PATHL))
     1-(R1*R1/2.-R1*R1*R1/(3.*PATHL)))
      TERMV=4.6*SQRT(DMODE)
      DROPS=531.*RATE/(TERMV*DMODE*DMODE*DMODE)*VOLUME
      MINUSJ=CMPLX(0.,-1.)
      S11=0.5*MINUSJ*F11*DROPS*2.*(2./3.14159)/R
      S22=0.5*MINUSJ*F22*DROPS*2.*(2./3.14159)/R
      S12=0.5*MINUSJ*F12*DROPS*P*2.*(2./3.14159)/R
      J=N
      EM=(1.+S11)**J
      E=CMPLX(0.,0.)
      DO 2 I=1,J
      K=J-I
      L=I-1
      E=E+(1.+S11)**K*(1.+S22)**L
    2 CONTINUE
      EX=E*S12
      EMR=REAL(EM)
      EMI=AIMAG(EM)
      EXR=REAL(EX)
      EXI=AIMAG(EX)
      EMMAG=SQRT(EMR*EMR+EMI*EMI)
      EMPHAS=ATAN2(EMI,EMR)
      EMPHAS=EMPHAS*57.295
```

```
   EMDB=20.*ALOG10(EMMAG)
   EXMAG=SQRT(EXR*EXR+EXI*EXI)
   EXPHAS=0.
   IF(EXMAG.EQ.0.)GO TO 9
   EXPHAS=ATAN2(EXI,EXR)
   EXPHAS=EXPHAS*57.295
   EXDB=20.*ALOG10(EXMAG)
   EXPOL=EXDB-EMDB
 9 THETA=THETA*57.295
   WRITE(6,12)PATHL,RATE,THETA,N,P
12 FORMAT(1HO,'PATHL=',F8.2,5X,'RATE=',F8.2,5X,'THETA=',F8.2,5X,'N=',
  1F8.2,5X,'P=',F8.2)
   WRITE(6,3)EMMAG,EMPHAS,EXMAG,EXPHAS
 3 FORMAT(1HO,'EMMAG=',F10.5,5X,'EMPHAS=',F10.5,5X,'EXMAG=',F10.5,5X,
  1'EXPHAS=',F10.5)
   IF(EXMAG.EQ.0.)GO TO 10
   WRITE(6,4)EMDB,EXDB,EXPOL
 4 FORMAT(1HO,'EMDB=',F10.5,5X,'EXDB=',F10.5,5X,'EXPOL=',F10.5)
   GO TO 13
10 WRITE(6,11)EMDB
11 FORMAT(1HO,'EMDB=',F10.5)
13 WRITE(6,8)
   WRITE(6,8)
   WRITE(6,8)
 8 FORMAT(1HO)
   GO TO 6
 5 STOP
   END
```

Important variables in the above program are:

PATHL - Path length in meters

RATE - Rain rate in mm/hr

THETA - Tilt angle of incident polarization in degrees

N - Number of path segments (must be even)

ALPHA - Tilt angle of cross polarization in degrees

P - Fraction of effective oblate drops

DMODE - Most frequently occurring drop size (Empirical fit to Laws and Parson's data)

FVR - Real part of single drop scattering function for vertical polarization (Empirical fit to Oguchi's data)

FVI - Imaginary part of above

FHR - Real part of single drop scattering function for horizontal polarization (Empirical fit to Oguchi's data)

FHI - Imaginary part of above

FV - Oguchi's scattering function for vertical polarization

FH - Oguchi's scattering function for horizontal polarization

F11 - Scattering function, incident to incident polarization for one drop

F12 - Scattering function, incident to cross polarization for one drop

F22 - Scattering function, cross to cross polarization for one drop

R - One-half the path length

VOLUME - Volume of a segment of the path bounded by the first Fresnel zone

TERMV - Terminal velocity of raindrops [8]

DROPS - Number of drops of size DMODE in VOLUME

S11 - Scattering function, incident to incident polarization for one plane of drops

S12 - Scattering function, incident to cross polarization for one plane of drops

S22 - Scattering function, cross to cross polarization for one plane of drops

EM - Received signal, incident (main) polarization

EX - Received signal, cross polarization

EMMAG - Magnitude of received signal, incident polarization

EMPHAS - Phase of received signal, incident polarization

EXMAG - Magnitude of received signal, cross polarization

EXPHAS - Phase of received signal, cross polarization

EMDB - Received signal in dB, incident polarization

EXDB - Received signal in dB, cross polarization

EXPOL - Cross polarization level in dB

The convergence of the above program as N is increased is shown in Figure A-3 where the cross polarization level is shown for a path length of 1.43 km, a rainrate of 150 mm/hr, a frequency of 19.3 GHz, and a tilt angle of 45°. As can be seen, convergence to within 1 dB of the final value is obtained for N=20.

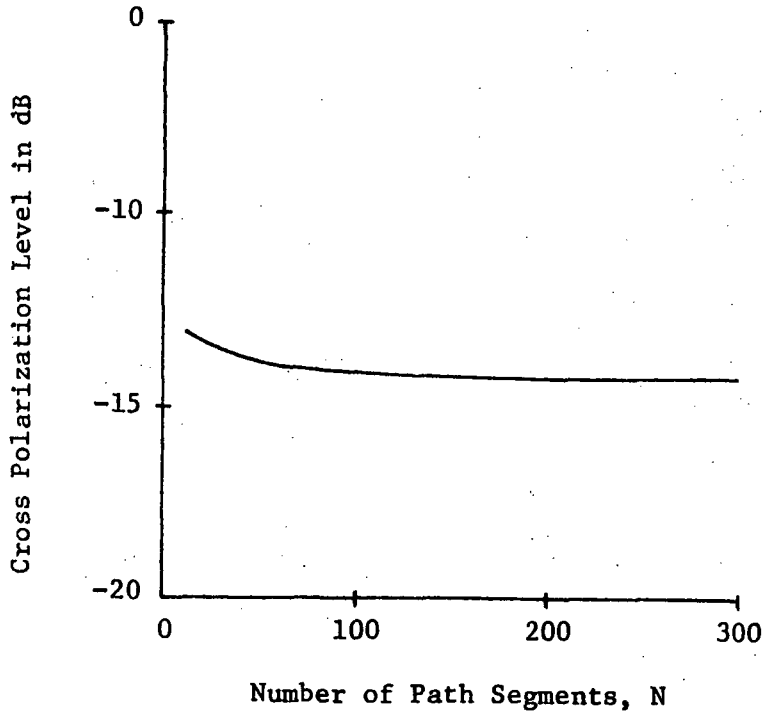


Figure A-3. Convergence of the Model as the Number of Path Segments is Increased.